Fission Gas Behavior in Nuclear Fuels

A Thesis Presented for the

Master of Science

Degree

The University of Tennessee, Knoxville

Abdullah Maki Alani

May 2020

ACKNOWLEDGEMENTS

First, I would like to thank my advisor, Dr. Brian Wirth, for his guidance and mentorship during my time at the University of Tennessee. I first met Dr. Brian Wirth when I was an undergraduate student, and he taught the introduction to nuclear engineering course. His teaching method inspired me to strive to do better, whether by encouraging me and all other students to participate more during class time or by his excellent selection of challenging assignments which helped me develop a researcher's mentality at a very early stage in my academic endeavors. I am grateful for the opportunity you gave me to work under your advisement—it helped me grow as a student, researcher, and will hopefully carry on in my professional life as an engineer.

I would also like to thank Dr. Heilbronn, Dr. Maldonado, and Dr. Zinkle, for being exceptional teachers who taught me the fundamentals of nuclear engineering. I appreciate you taking the time to be a part of my thesis committee.

Dr. Sophie Blondel, thank you for all the help you provided during the time I worked on this project. Your prompt responses and code development have been of tremendous help.

A special thanks to Dr. Jamie Coble, who always supported and encouraged me. During class, you went the extra mile to ensure everyone had a good grasp of all the topics you taught, and you did the same as the advisor of my undergraduate senior design project. I am honored to have met and worked with an exemplary engineer such as yourself.

Last but not least, my family and friends. Words cannot describe how much support my parents have shown me throughout my life. You shaped me into being who I am today, and I would not have made it to this point without you. You two are prime examples of loyalty, courage, and dedication. I am proud to have you as parents. As for my siblings, I still look up to the older ones, while the little ones are the source of my strength to keep moving forward in hopes to always make them proud. I honestly do not know what to say about my friends, they were not very helpful. Jokes aside, I appreciate and love you all, even if I do not show it often.

ABSTRACT

The purpose of this thesis is to provide an overview of fission gas behavior in nuclear fuels, specifically Xe and Kr gas bubble evolution in UO_2. This is important due to the fact that the diffusion of these noble gases and their precipitation directly affect fuel swelling and gas release to the fuel rod plenum, which impacts fuel performance. The mechanisms of how fission gas bubbles are formed in the fuel and fission gas release are discussed in three stages—Xe and Kr diffusion and trapping by intra-granular bubbles, followed by bubble nucleation and coalescence on grain faces, and finally the escape/release of fission gas through the interconnected grain boundaries. Intra-granular fission gas bubble evolution is investigated in this research, to provide a better understanding of their behavior in order to eventually devise a more accurate model that better agrees with experimental data. The proposed approach to construct a new model includes using the Xolotl-Fission code, which serves as a solver for reaction-diffusion equations and incorporates atomistic mechanisms. The parameters used in Xolotl are based on previous studies that are thoroughly investigated in the background section of the thesis. Some of the experiments mentioned in the literature review, such as temperature sensitivity analysis and annealing experiments, are replicated using Xolotl. The results are then compared to the experimental data and then provide feedback for the development and improvement of Xolotl or, if accurate, confirm the results of the experiments. Current results show that calculations obtained utilizing Xolotl underestimate the average number density of bubbles, while overestimating the average radius of bubbles compared to literature.

TABLE OF CONTENTS

Chapter One: Introduction and General Information 1

1.1 Purpose 1

1.2 Thesis Outline 2

Chapter Two: Background and Literature Review 4

2.1 Stage 1: Xe Diffusion and Trapping by Intra-Granular Bubbles 4

2.2 Stage 2: Bubble Nucleation and Coalescence on Grain Faces 6

2.3 Stage 3: Release of Fission Gas through Interconnected Grain Boundaries 7

2.4 Literature Review 7

Chapter Three: Methods and Modeling 20

3.1 Model Setup 20

3.2 General Information and Current State of Xolotl 20

3.3 Xolotl Input Parameters and Output Files 21

Chapter Four: Results and Discussion 23

4.1 Sensitivity Analysis Without Re-solution 23

4.2 Effects of Implementing Re-solution 24

4.3 Sensitivity Analysis With Re-solution 28

4.4 Bimodal Distribution 29

4.5 Diffusion Coefficient 32

4.6 Annealing 35

Chapter Five: Conclusions and Recommendations 39

List of References 40

Vita 44

LIST OF FIGURES

Figure 2.1: Images showing the formation, growth, and nucleation of inter-granular bubbles 6

Figure 2.2: TEM images of irradiated samples, as reproduced by Baker [7] 11

Figure 2.3: TEM image of samples irradiated to different burnups, at 1073 K, as reproduced by Kashibe [8] 12

Figure 2.4: Turnbull's analysis of unirradiated polycrystalline materials under isothermal conditions 15

Figure 2.5: Diffusion coefficients as a function of reciprocal temperature 16

Figure 2.6: Xenon diffusion coefficient values from multiple sources, as reproduced from Ref. [13] 18

Figure 2.7: In-pile diffusion coefficients depending on temperature, as reproduced from Ref. [13] 18

Figure 4.1: Plot of average radius plotted against time of various temperatures selected based on Cornell *et al.* [6] 23

Figure 4.2: Xenon bubble distribution obtained by simulating a fission rate density of 8e18 fissions/nm3/s with operating temperature of 1073 K for 23, 44, and 83 GWd/t burnups 24

Figure 4.3: Heterogeneous re-solution rate as a function of the percentage of effective electronic stopping power taken as thermal spike. 25

Figure 4.4: Xe bubble size distribution for different values of thermal spike 26

Figure 4.5: A plot showing the effects of increasing the percentage of stopping power that is taken as thermal spike Z on the average radius over time. 26

Figure 4.6: Plot showing the effects of varying the reaction radius on re-solution rate 27

Figure 4.7: Average radius of bubbles with radius bigger than 0.7 nm at different temperatures with and without re-solution. 29

Figure 4.8: Xe bubble distribution after using an artificially created bimodal distribution with concentration peaks at 200 and 3000 Xe atoms 30

Figure 4.9: Xenon distribution after starting with an artificially created bimodal shape . 31

Figure 4.10: Xenon distribution as a result of varying re-solution 32

Figure 4.11: Effects of diffusion on the size distribution for different temperatures 34

Figure 4.12: Xolotl plots based on Kashibe experiment [8] where a sample is irradiated to 23 GWd/t..... 36

Figure 4.13: Xolotl plots based on Kashibe experiment [8] where a sample is irradiated to 44 GWd/t..... 36

Figure 4.14: Xolotl plots based on Kashibe experiment [8] where a sample is irradiated to 83 GWd/t..... 37

Figure 4.15: Annealing test results obtained using Xolotl..... 38

CHAPTER ONE

INTRODUCTION AND GENERAL INFORMATION

1.1 Purpose

The objective of this research is to investigate the fission gas behavior in nuclear fuel through performing sensitivity analysis based on experimental data obtained from literature. In order to do that, the Xolotl-Fission code is utilized, coupled with the powerful computational capabilities of the University of Tennessee, Knoxville Advanced Computing Facility (ACF). The results of the sensitivity analysis also provide feedback to improve the Xolotl-Fission code, in order to achieve higher accuracy, more efficiency, and add changes to improve current and future users' experience. The importance of the development of a code such as Xolotl-Fission lies in its ability to provide information about nuclear fuel performance that is otherwise impractical to obtain during reactor operation. Accurate simulations of fuel performance potentially lead to attaining better fuel utilization through higher burn-ups, reduce unexpected and expected outages for refueling, and higher accident tolerance.

The aforementioned research goals are carried out by understanding the mechanisms of gas bubble formation in nuclear fuel through modeling the stages that lead to fission gas release from the fuel. The goal of the fission gas behavior model is to account for three spatially-dependent quantities that happen at different irradiation times: the concentration of gas atoms within the fuel matrix; the number of gas bubbles in the matrix, on dislocation lines, and on grain boundaries; and the amount of gas released from the fuel. These quantities must add up to the gas that is produced by fission. The model should also include the three stages that the fission gases go through before escaping to the fuel rod free volume. Stage one involves fission gas production and intra-granular bubble formation. Stage two involves the nucleation, growth, and interconnection of inter-granular bubbles. And stage three is when the fission gas escapes to the fuel rod free volume by travelling through the tunnels formed by the interconnection of grain edges.

In order to model the fission gas behavior in nuclear fuel, multiple scales must be considered. From the nano-scale of fission gas formation and bubble nucleation to the centimeter-scale of the fuel pellets, a meso-scale model is to be constructed to capture all stages

that lead to fission gas release. And since these three stages happen at different irradiation times, noting that they can occur simultaneously, the model must also be multi-time scaled. This helps in obtaining more accurate results with lower uncertainties. Powerful computational tools are used to simulate at least a few hundred particles in order to get less biased results and more reliable data. The Xolotl-fission code is used in this research to describe the evolution of intra-granular bubbles. The gas heterogeneous re-solution from bubbles back to the fuel has been recently implemented in the code, which provides a better understanding of the true mechanisms of fission gas behavior with less uncertainty, unlike previous models.

The fission gas behavior in nuclear fuel is very important to both industry and DOE-NE research. This is due to the fact of it having the biggest impact on the fuel performance, and how it can possibly result in the fuel's failure. Thus, many models have been developed over the years in order to get a better understanding and more accurate predictions of the Xe and Kr gases' behavior in the fuel. As mentioned before, the fission gas bubble production and gas release comprise of three stages. Stage one being fission gas (Xe,Kr) diffusion and trapping in intra-granular bubbles; stage two is the bubble interconnection on grain faces; and stage three is the release of fission gas through interconnected bubbles on grain edges. All these stages can happen simultaneously, though they are governed by the time at which stage one occurs at the beginning. They are all impactful contributors to the eventual gas release, and must all be modeled to produce reliable predictions. However, older models exclude the last stage before gas release, and assume that all the gas in the bubbles is released after reaching a threshold. They also rely heavily on empirical potentials and density functional theory (DFT) calculations which come with high uncertainties. This results in oversimplified models that are inaccurate, or at least not accurate enough to base important enhancement efforts of nuclear fuel performance upon them. In this research, an atomistic-informed approach is considered while simulating the behavior of fission gas intra-granular bubbles.

1.2 Thesis Outline

Background information related to the work done and presented in this thesis is found in Chapter Two. That chapter also includes an overview of several past experiments and developed models relating to the topic of fission gas behavior in nuclear fuel. Chapter Three represents the

overall setup of the modeling process, and how Xolotl-Fission is utilized in order to obtain the results presented in this thesis. Some of the available parameters in Xolotl-Fission are listed and described in Chapter Three. The results obtained using Xolotl-Fission are presented and discussed in Chapter Four, along with comparisons to past research efforts. Finally, conclusions are drawn in Chapter Five, in addition to recommendations for future research based on the results presented in this thesis.

CHAPTER TWO

BACKGROUND AND LITERATURE REVIEW

The behavior of fission gases, particularly xenon and krypton, in nuclear fuel is important because of how it affects the fuel performance during normal operation and transient conditions. They are noble, insoluble gases, making it relatively easy for them to be rejected from the fuel matrix. In addition to that, the pure state of Xe and Kr is gas, which makes them follow one of two paths upon rejection—they are either released to the fuel pins, or precipitate to form gas bubbles within the fuel. Both of these cases are of critical importance to fuel performance. In the case where they are released, they increase the pressure within the fuel pins, resulting in an increased risk of fuel cladding failure due to high stress. On the other hand, when Xe and Kr gases precipitate in the fuel and form gas bubbles, they increase fuel swelling which increases the contact of the fuel and the cladding. This causes the stress on the cladding to rise, which results in shortening its lifetime. Another problem with gas being retained as bubbles within the fuel is the fact that the temperature of the fuel increases due to its reduced thermal conductivity.

The goal of a fission gas behavior model is to account for three spatially-dependent quantities that happen at different irradiation times: the concentration of gas atoms within the fuel matrix; the number of gas bubbles in the matrix, on dislocation lines, and on grain boundaries; and the amount of gas released from the fuel. These quantities must add up to the gas that is produced by fission [1]. The model should also include the three stages that the fission gases go through before escaping to the fuel rod free volume. Stage one being the fission gas production and intra-granular bubble formation. Stage two notes the nucleation, growth, and interconnection of inter-granular bubbles. And stage three is when the fission gas escapes to the fuel rod free volume by travelling through the tunnels formed by the interconnection of grain edges [2]. The focus of this research is Xe behavior in nuclear fuel rather than Kr.

2.1 Stage 1: Xe Diffusion and Trapping by Intra-Granular Bubbles

The diffusion of fission gas atoms in bulk UO_2 is the first step of the whole process before gas release. Every other subsequent process is dependent on the bulk diffusion rate, making it very important to understand and accurately model. The bulk diffusion is temperature-

dependent and must be studied and modeled at different reactor conditions. The microstructural changes in the fuel must also be considered at different times in this stage. According to Turnbull *et al.* [4], the diffusivity is divided into three regimes depending on the temperature and stoichiometry. The first being the high temperature region (T > 1650 K) where intrinsic diffusion is the dominant process. In this region, it is believed that the noble gas atoms (Xe) occupy the sites of vacant anion and cation clusters. The intrinsic diffusion is defined by the motion of these clusters in a stoichiometric environment and at small concentrations of gas atoms. The second is the intermediate temperature region (1381 < T < 1650 K) where the radiation-enhanced diffusion process dominates, and the diffusivity is controlled by the fission rate where the cation vacancy concentration is enhanced due to irradiation damage. Lastly, the third region is the low temperature region (T < 1381 K) where the diffusion is virtually independent of temperature and is proportional to the fission rate only [2,3,4]. After the analysis of these regions, the unperturbed Xe diffusion coefficient D through UO_2 bulk is derived. This coefficient does not account for the trapping of Xe in intra-granular bubbles or other defects, nor does it account for the re-solution of the gas out of the bubbles. From that, the effective diffusivity of Xe is derived:

$$D' = \frac{D\, b'}{b'+g} \tag{1}$$

Where D' is the effective diffusivity, D is the unperturbed Xe diffusivity, b' is the re-solution of Xe into small intra-granular bubbles, and g is the trapping rate. The two latter parameters represent the role of fission gas release in intra-granular bubbles, which is important as it greatly impacts the gas diffusion to grain boundaries. The growth of the fission gas bubbles happens due to the migration of vacancies and fission gas atoms to the already existing bubbles that have formed via the clustering of gas atoms or their combination with defects. Since the growth of the bubbles is dependent upon vacancy migration and fission gas production rate, it is considered as a relatively slow process. The Xe atoms travel accompanied by uranium vacancies as a cluster. For instance, if a Xe atom is clustered with two U vacancies and this cluster is trapped in a bubble, the bubble grows by two vacancies. Results from Andersson *et al.* [3] show that the Xe atom is usually accompanied by two vacancies, but results from the NE-SciDAC 2 proposal show that the most stable form would be six or eight U vacancies that cluster with the Xe atom [2]. That being said, vacancy migration and clustering with Xe atoms is yet to be implemented in Xolotl. Observation made by Cornell [6] and Baker [7] indicate that as the irradiation

temperature increases, the number density of the bubbles experiences a general decreasing trend while the size of the bubbles increases in this stage. This is in accordance with what is provided by G. Was [5], and will be discussed in further detail later in this thesis.

2.2 Stage 2: Bubble Nucleation and Coalescence on Grain Faces

As intra-granular bubbles grow, they can come in contact with each other and eventually interconnect on grain faces. The shape that is formed by the interconnection is lenticular. Then, as more fission gas gets trapped in the bubbles, that lenticular shape is elongated and eventually gets linked to the grain edges, creating cigar-shaped bubbles. This is shown in Figure 2.1 below. The resulting interconnection creates a path for the fission gas atoms to escape to grain boundaries [2]. In earlier investigation of fission gas behavior in nuclear fuel, a threshold is chosen at which all the trapped gas is released from grain faces to grain boundaries. That threshold is characterized by the ratio of fission gas bubbles to the spherical grain boundary that it covers, and is typically chosen to be 50%. This assumption results in high uncertainties, because some of the Xe gas atoms escape before or after reaching the proposed threshold of 50%.

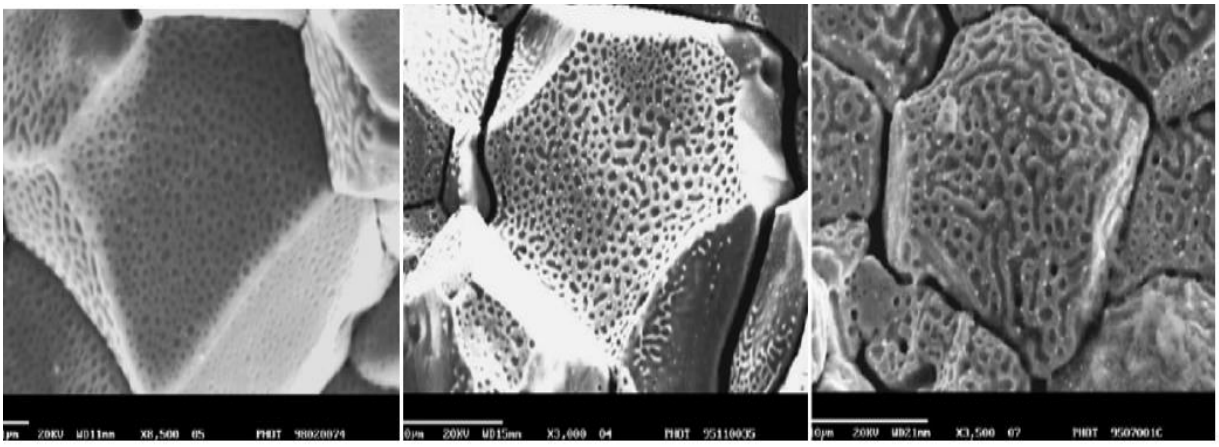


Figure 2.1: Images showing the formation, growth, and nucleation of inter-granular bubbles. Left most image shows early stage of early stage of grain boundary swelling at a burnup of about 13 GWd/t. The center image shows moderate grain boundary porosity at about 21 GWd/t burnup. The right most image shows grain boundary porosity at 21 GWd/t burnup, but with annealing at 1800 °C for 30 minutes, as reproduced from Ref. [8].

2.3 Stage 3: Release of Fission Gas through Interconnected Grain Boundaries

This stage has been ignored by most previous fission gas behavior models due to the high computational costs and lack of modeling capabilities that capture its complication. In this stage, after the inter-granular bubbles interlink with the grain boundaries, the shape of the bubbles turns into tunnels at the grain edges for the gas to be released. These tunnels have considerably longer length than the lenticular bubbles at the grain faces. However, due to the high surface tension, these tunnels collapse resulting in the fission gas atoms to flood back to the grain faces. This process happens iteratively, each time making the tunnels longer and more resistant to pressure until they eventually stabilize, creating a path for the fission gas atoms to be released from pores in the grain boundaries into the free volume of the fuel rod [2].

2.4 Literature Review

One of the earliest efforts to understand the fission gas behavior in nuclear fuel is the work done by Booth *et al.* back in 1957 [12]. The goal of that research is to calculate the fraction of fission gas that diffuse out of the nuclear fuel (UO_2) under reactor conditions. The study is done relying on diffusion coefficients that are determined numerically through a lab experiment, based on the assumption that the values of these coefficients remain unchanged in a reactor. For instance, it is assumed that the diffusion geometry is unaffected by the changes that happen to the fuel during operation. Other assumptions are made about the temperature of the fuel, which adds to the uncertainty of the results significantly. The accuracy of the calculations is hindered by the inability to precisely determine the irradiation temperature of the fuel sample, due to the lack of knowledge about the degree that thermal expansion affects the gap between the fuel and the cladding. Finally, the geometry of the bubbles in this diffusion system is considered to be ideal, uniform spheres throughout the entire diffusion process. Based on these assumptions, the fraction of the fission gas that diffused out of the fuel at the end of the irradiation process is calculated and compared to experimental results. The experiment done to measure the rare gas that escaped the fuel is simple—after the fuel element is removed from the reactor, it is put in vacuum and the cladding is punctured in order to collect the stable gas atoms and measure them volumetrically. This adds yet another uncertainty, as Booth stated, due to some rare gas atoms possibly escaping the measurement. That happens because some of these gas atoms get trapped

in the fuel's free volume. One way to ensure a lesser degree of uncertainty due to trapping is to heat up the fuel sample after its removal from the reactor, in order to liberate all or most of the trapped rare fission gas atoms. The results show disagreement between the model and the experimentally collected data, where the fraction of rare fission gas that diffused out of the fuel was calculated to be 42-53%, while it was experimentally measured to be 5.3-5.7%.

Another early effort to understand the fission gas mechanisms and bubble behavior was done by Speight, presented in two papers back in 1964 [38,39]. In his studies, Speight suggests that bubble growth occurs due to the mobility of the bubbles and their subsequent coalescence. The bubbles move through a temperature gradient, or through surface diffusion of bubbles. This movement is halted in the presence of solid precipitates, unless re-solution occurs and dominates. In the case where bubbles of radius r_m are in equilibrium (surface tension is equal to bubble pressure), the velocity of the bubbles is the sum of the velocities from both mechanisms. In an environment where a temperature gradient is affecting gas bubbles with radius bigger than r_m, the bubbles move up the gradient due to a vapor transport mechanism with a velocity directly proportional to the radius. On the other hand, when the radius is smaller than r_m, the bubbles move due to surface diffusion of atoms surrounding the bubbles with a velocity that is inversely proportional to the radius.

Four years later, a study by Cornell *et al.* [6] was done to examine base irradiated materials in order to evaluate the role of bubbles in fission gas release, and the importance of the mobility of those bubbles. In this paper, a comparison between bubble mobility and evolution in out-of-pile experiments as opposed to behavior in reactor fuel is brought to light. For out-of-pile experiments done by Cornell and Williamson [32], and one by Manley [33], both results agree on the dependence of bubble velocity upon the inverse value of the radius (R^{-1}), despite significant differences in bubble evolution. In the latter experiment done by Manley, the results suggest that bubbles containing solid fission products were less mobile than bubbles that are not associated with precipitates. However, results from Barnes and Mazey [35] show that there is no correlation between bubble radius and velocity. They attribute that to significant deviation from stoichiometry. Another out-of-pile study done by Cornell and Bannister [36] suggests that the bubble radius is directly proportional to the velocity. However, the experiment in this study is conducted differently, where a UO_2sample is annealed at a constant temperature. This approach

interested Gulden who conducted a similar experiment [26] and found contrasting results. The findings of Gulden show that the velocity is related to the radius as $R^{-3/2}$, which suggests that the process's rate is controlled by volumetric diffusion. Another significant difference is the fact that the migration distance is 400 times lower compared to distances calculated assuming surface diffusion. As explained by Cornell [6], the only significant difference between the two experiments is the material used, where Cornell and Bannister injected the gas atoms as ions, while the sample used in Gulden's experiment is an irradiated reactor fuel sample. In the latter experiment, significant precipitation occurred, and hindrance of bubble motion could be attributed to that. A final study by Walker [30] is mentioned by Cornell to conclude this investigation. Walker's result show similar trends to the study done by Cornell and Bannister, except for bubbles with radius above 10 Angstroms—after reaching that size, the velocity of the bubbles start to decrease with increasing radius. Finally, due to the vast differences seen in all the previously mentioned studies, the results are deemed inconclusive when it comes to the relationship of bubble radius and velocity, and bubble mobility in general.

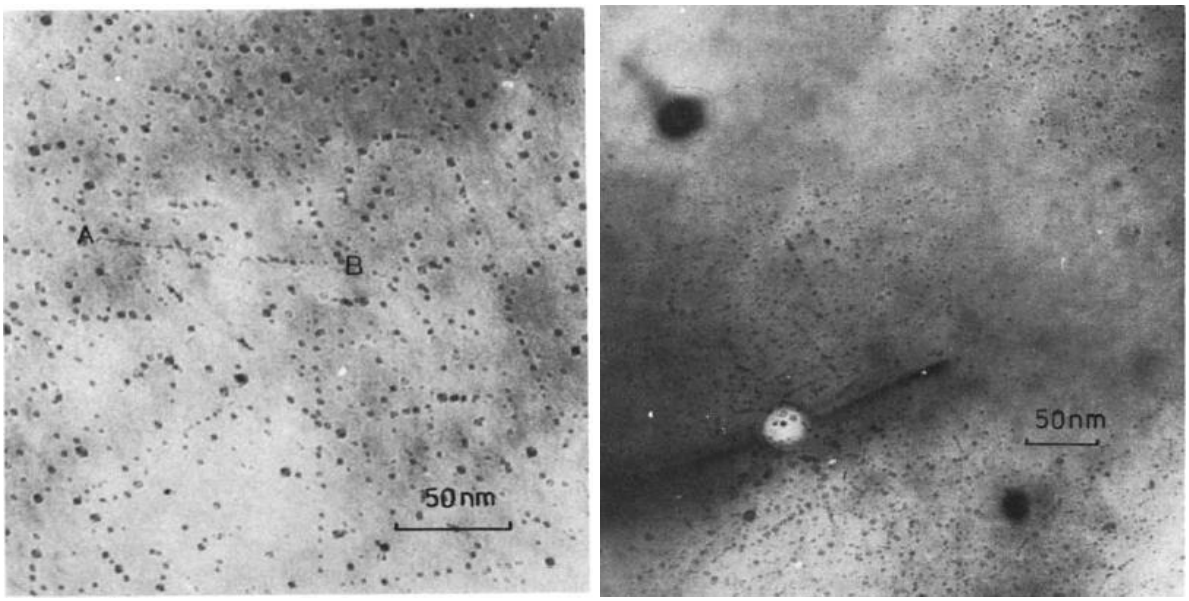
Further investigation of bubble behavior in fuel was done by Cornell. An experiment was conducted where irradiated uranium dioxide thin foil samples are prepared after reaching a burnup of $3.2 * 10^{25}\ fissions/m^3$ in 40 days, with an estimated irradiation temperature range of 860-1580 ℃. The bubble concentration, diameter, and atom concentration in the bubble were measured for each temperature, and are shown in Table 1. As noted by Cornell, the difference in bubble concentrations and diameters at different temperatures is not significant, suggesting that the bubbles do not migrate through the temperature gradient mechanism. This lack of mobility is attributed to either precipitates restraining the bubbles and preventing them from moving, or a very small surface diffusion rate. That being said, the volume diffusion mechanism cannot be excluded. In that case, the small bubbles will be unaffected by the temperature gradient and will move at random due to the Brownian motion. The bubbles that initially precipitate have high concentrations. That fact coupled with random motion of these bubbles results in a high number of bubble-bubble interactions, which lead to numerous coalescence events. As bubbles coalesce, they grow bigger which hinders their mobility due to the nature of the relationship between bubble velocity and volume in the volume diffusion mechanism—the velocity is proportional to $R^{-3/2}$. This leads to large bubbles that keep increasing in size rather than traveling to grain boundaries.

Table 1: Intra-granular bubble size and density as a function of irradiation temperature as reproduced from Ref. [6].

Temp. (°C)	Bubble conc. (no./m³)	Bubble dia. (Å)	Total atom conc. (no./m³)
1580	1.18×10^{23}	28	1.31×10^{25}
1570	1.24×10^{23}	26	1.12×10^{25}
1510	1.32×10^{23}	24	0.95×10^{25}
1470	1.83×10^{23}	23	1.17×10^{25}
1425	2.46×10^{23}	20	1.06×10^{25}
1270	2.90×10^{23}	20	1.25×10^{25}
1060	3.30×10^{23}	19	1.25×10^{25}
980	3.50×10^{23}	18	1.16×10^{25}
860	3.80×10^{23}	17	1.06×10^{25}

Such mechanism will not work in a model that is devised to estimate the quantity of gas atoms that transfer to the grain boundaries, and the rate of that transfer, and it is concluded that single atom diffusion is needed for gas atoms to reach grain boundaries. Thus, another mechanism is needed where intragranular bubbles still exist, but are accompanied by single gas atoms, and that mechanism is called re-solution. An outline of a re-solution model is discussed in this paper, where the re-solution is independent of bubble radius, and can be calculated empirically through observation of intragranular bubble behavior in experimental data, rather than a mechanistic approach.

Baker [7] expands on work done by Cornell by examining the same temperature range, and adding further insight as to what happens when the temperature is increased beyond 1600 C. One of the first remarks by Baker is the confirmation of the hypothesis that bubbles form on dislocations and fission fragment tracks. This observation is made clear above 1000 C, and as temperature increases, the lines of bubbles begin to become longer and are easier to identify, as seen in Figure 2.2 (a). Above 1700 C, the uniformity of gas bubble distribution is disrupted,



a) b)

Figure 2.2: TEM images of irradiated samples, as reproduced from Baker [7]. a) TEM image of a sample with irradiation temperature 1650 ℃. Line AB denotes what looks like a forming dislocation decorated with bubble nucleation in a line. b) TEM image of the same sample at 1800 ℃ irradiation temperature, showing areas devoid of bubbles, while a large concentration of small bubbles located near bigger bubbles that nucleated on dislocations.

where more bubbles start to nucleate near grain boundaries. As seen in Figure 2.2 (b), there are areas with no bubbles, while the concentration of small bubbles increases around the big bubbles that nucleate on dislocations. Baker then compares his work to Cornell, where experiments done by Baker in the same temperature range result in smaller bubbles with higher density, and attributes that to better foil preparation and a more accurate method of measuring the bubble radius. These authors, however, reach the same conclusion that the bubble radius is only weakly dependent on irradiation temperature, which leads to the belief of irradiation enhanced diffusion. Finally, Baker confirms the lack of evidence of intra-granular bubble mobility.

A more recent study of fission gas behavior in nuclear fuel was published by Kashibe *et al*. [8] in 1993. The paper highlights the effects of reaching higher burnup values and the results of annealing of the irradiated uranium dioxide fuel samples. TEM imaging is used to study the behavior of bubbles at different burnups. As seen in Figure 2.3, small bubbles that are 2.2 nm in

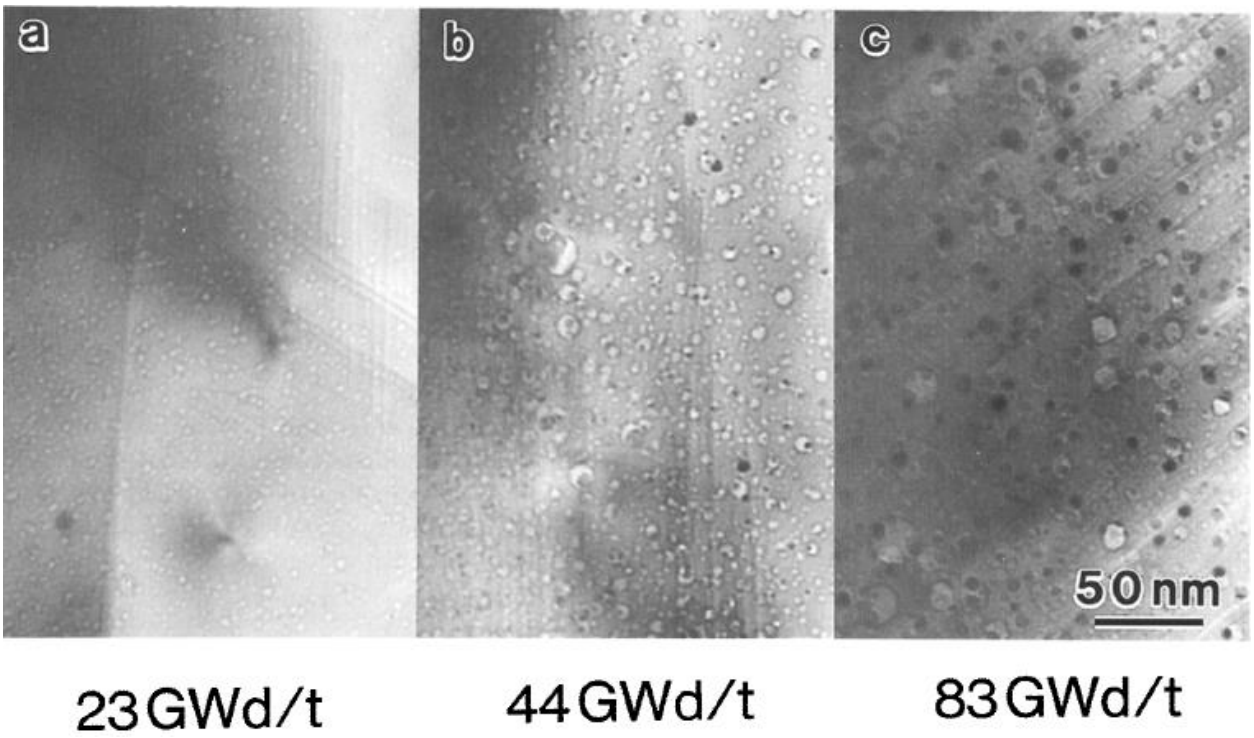


Figure 2.3: TEM image of samples irradiated to different burnups, at 1073 K, as reproduced from Kashibe [8].

diameter appear in all burnup conditions. However, as the burnup is increased to the middle range of 44 GWd/t and the high range of 83 GWd/t, new bubbles with larger size (10-20 nm diameter) appear. Increasing burnup results in the overall increase of the average bubble sizes, and a slight decrease in the mean concentration, though the concentration of the bigger bubbles increases.

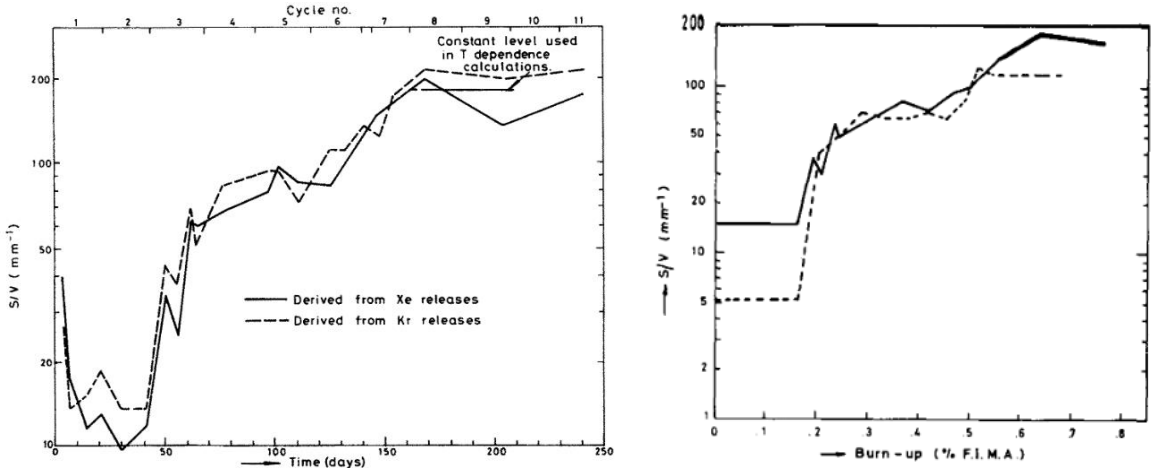
Finally, Kashibe *et al.* observe a shift in the bubble size distribution which goes from a mono-modal shape at low burnup to a bimodal shape at high burnups. They attribute the bimodal shape to either coalescence of small bubbles, or vacancy capture into bubbles that contain solid fission products. Results from Baker [7] appear to be in agreement compared to results obtained by Kashibe in fuel that irradiated to 23 GWd/t burnup. On the other hand, comparisons to Ray et al. [28] show a discrepancy in density calculations. In the experiment by Ray, only the bigger bubbles of 8 nm diameter are observed for fuel at 44 GWd/t burnup, and thus the calculated density is lower due to the fact that the density of 2 nm bubbles is not accounted for.

Kashibe *et al.* also discuss the effects of annealing, where fuel samples of 23, 44, and 83 GWd/t are annealed at 1800 ℃ for five hours. When the 23 GWd/t sample is annealed, coarsening occurs near the grain boundaries and the bubbles increase in size to about 3 microns, while no smaller bubbles are observed. However, bubbles have a smaller size of 44-55 nm in the grain interior. The coarsening can be attributed to vacancy migration through interconnected grain boundary tunnels, which can explain why this effect is not seen in the central region of the grain, since most vacancies will not be able to travel that far of a distance from the grain boundaries to the interior of the grain. For the annealing of 44 and 83 GWd/t burnup fuel samples, the smaller bubbles (44-55 nm) are not observed at the center of the grain. Rather, the size of the bubbles at the center of the grain is between 100 nm and a micron. It is also confirmed that smaller bubbles below several 10 nm are not observed. Finally, the coalescence of bubbles is observed after the annealing of 83 GWd/t fuel, where two bubbles seem to connect and form a single bubble that is peanut-shaped.

The diffusion calculations based on temperature regimes mentioned in this thesis, particularly in stage one of gas bubble evolution, come from the work of Turnbull *et al.* [4]. In that work, an extensive study is done in order to construct a comprehensive model to calculate the diffusion coefficients of different gases in uranium dioxide under irradiation. In order to ensure that the fission rate is unaffected by fission events from plutonium, the fuel samples used in the experiment are enriched to 20% U-235. In order to get to that level of enrichment, a method devised by Robins [22] is used, where single uranium dioxide crystals are grown by doping uranium dioxide powder with a melt of sodium and potassium chloride. The UO_2 powder is in the form of a mixture of natural enrichment and 93% enrichment. In addition to that, two polycrystalline samples of different origins are used in the experiment. Both samples have a grain diameter of about 10 microns and 20% enriched U-235. All the samples are irradiated with a constant neutron flux of $4 * 10^{16}\ neutrons\ m^{-2}s^{-1}$. Using an electrical heater, the temperature is held constant for seven cycles at 1400 C (for 157 days at full power). Then, the temperature is varied in a range between 225 and 1400 C for three more cycles. The fission gases are then collected, and Kr-85 was measured using beta-counting while the Xe-133 and Xe-135 were measured using gamma-counting. The measurements are then used to determine the release rate of iodine, xenon, bromine, and krypton. The effects of halogen precursors are resolved and diffusion coefficients are derived through Speight's analysis [15] coupled with the average

fractional release rate (R/B), where R is the release rate of gas atoms from the fuel and B is the generation rate of those gas atoms within the fuel. Data for single the crystals under isothermal conditions is analyzed for the first seven cycles at 1400 ℃. During that time, the crystals produced short-lived rare gases at an approximately constant rate. Also, knowing the weights of the crystals and the ability to measure their surface area optically makes it possible to derive a value of the surface to volume ratio ($\frac{s}{v}$). Knowing that $\left(\frac{s}{v}\right) = \left(\frac{3}{a}\right)$, where a is the effective sphere size, and using that in conjunction with release to birth ratios, it is possible to derive values for diffusion coefficients. Diffusion coefficients for xenon and iodine are derived, from the analysis of Xe-135 and Xe-138, with their values being $2.15^{3.0}_{1.5(5)} * 10^{-19}\ m^2\ s^{-1}$ and $2.5^{4.0}_{1.4} * 10^{-19}\ m^2\ s^{-1}$ for xenon and iodine, respectively. Krypton and bromine diffusion coefficients are also derived from analysis of Kr-85m, Kr-87, and Kr-88 during irradiation, resulting in $D_{Kr} = 7.9^{12.5}_{4.4} * 10^{-20}\ m^2\ s^{-1}$ and $D_{Br} = 1.50^{2.5(5)}_{0.83} * 10^{-17}\ m^2\ s^{-1}$. The limits shown indicate the maximum and minimum diffusion coefficients obtained using an effective sphere size displaced by $\pm$10%, and fractional release rate displaced by $\pm$7%, which means that they correspond to errors of one standard deviation in the measured data. Then, data for polycrystalline material is also analyzed for the first seven irradiation cycles at 1400 ℃. The results show that the polycrystalline materials that have been previously irradiated also produces gases at a constant rate in the first seven cycles of irradiation. From those results, and by using the diffusion coefficients of the single crystals, the surface to volume ratios are derived for xenon and krypton, with their values being $108\ mm^{-1}$ and $128\ mm^{-1}$, respectively.

Previously unirradiated polycrystalline materials were also investigated under the same isothermal conditions. Unlike single crystals and pre-irradiated polycrystalline, the results show that the unirradiated polycrystalline goes through significant increase in release during the first seven irradiation cycles. It was discovered that krypton and xenon behave very similarly when the values of their surface to volume ratios are compared, as can be seen in Figure 2.4 (a). An average line is then taken from these $\left(\frac{s}{v}\right)$ values, and is plotted along with data from a previous experiment done by Turnbull *et al.* [24] in Figure 2.4 (b), which shows significant similarities of the two experiments that indicate the "onset of open porosity occurring at the same burnup."

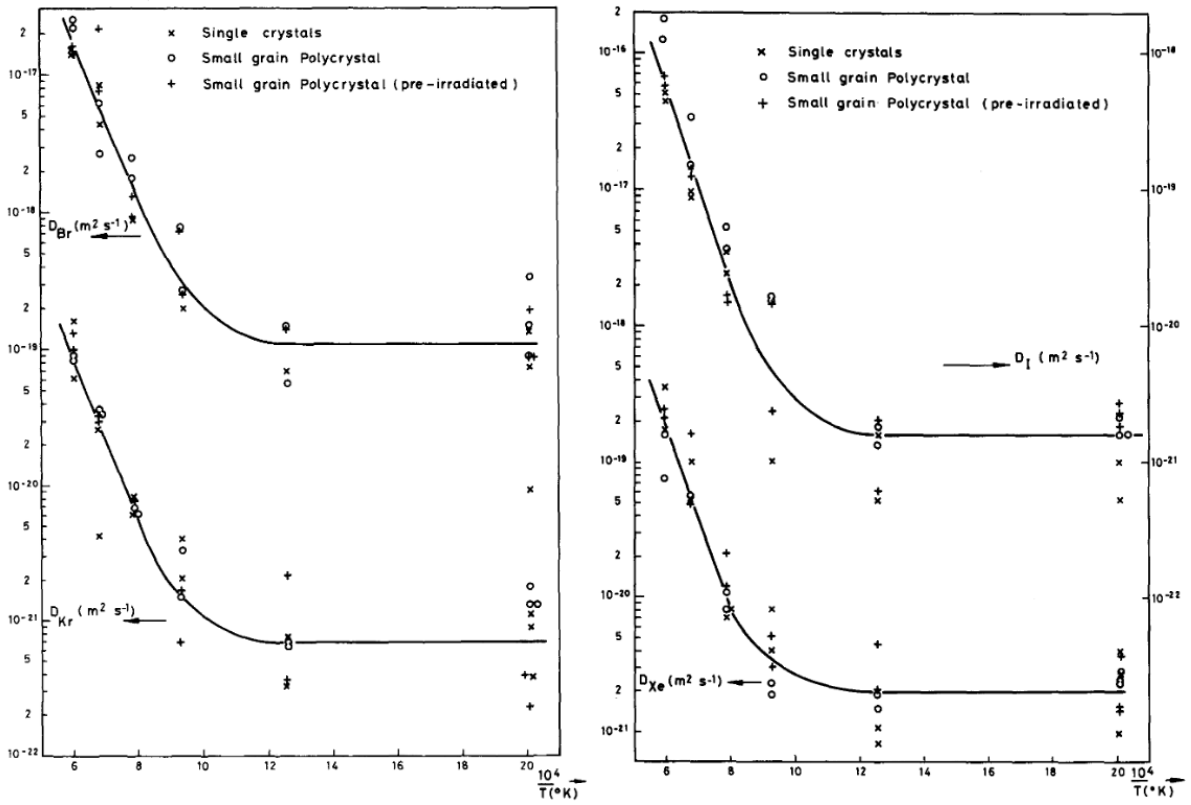


a) b)

Figure 2.4: Turnbull's analysis of unirradiated polycrystalline materials under isothermal conditions; a) Values of surface to volume ratio $(\frac{s}{v})$ derived from xenon and krypton release for unirradiated polycrystalline with diameter of ~10 microns under isothermal conditions with a temperature of 1400 ℃, plotted against irradiation time. b) $\left(\frac{s}{v}\right)$ values plotted against bum-up; ____ represents average line for specimens from (a), with rating ~33 W/gU; - - - - specimen of previous experiment [24] with rating ~12 W/gU. In both cases the initial stage is idealized [13].

After the first seven isothermal irradiation cycles, all samples reach "steady-state release of short-lived rare gases corresponding to stable microstructures," and data from three more cycles are used to investigate the effects of varying temperature, where multiple temperatures between 225 ℃ and 1400 ℃ are used. In order to measure $(\frac{R}{B})$, a period of constant temperature is necessary to achieve equilibrium release before each measurement. Then, diffusion coefficients are derived through the same Friskney and Speight analysis [37], and the results are plotted and shown in Figure 2.5.

The dependence of the gas release process on time and temperature is discussed in [13]. There are two cases of time dependence—one for stable isotopes and another for short-lived isotopes. For a longer-lived isotope, such is Kr-85, it is possible to collect atoms that are relatively far, because they have time to travel the distance despite the slow diffusion. That, however, depends



a) b)

Figure 2.5: Diffusion coefficients as a function of reciprocal temperature; a) values for krypton and bromine; b) values for xenon and iodine. As reproduced from Turnbull [13].

on the time of the experiment. On the other hand, unstable isotopes are constrained by their half-lives, where the generation, diffusion, and release must be on the order of the half-life rather than the experiment time. This means that the longer-lived isotopes have an "effective" diffusion coefficient D_s that depends on both temperature and time.

In a previous study done by Cornell and Turmbull [12], it was observed that a population of small intragranular bubbles exists after reaching burnups of $1.7 - 3.2 * 10^{25}\ fissions/m^3$, which corresponds to the burnup reached after cycle 1 in Turnbull's experiment [13], after which the bubbles' sizes and concentrations are affected by irradiation damage. The bubble size can be given by $R^4 = R_0^4 + (\frac{2\Omega_g YDt}{\pi r_f})$, where r_f is the fission fragment range in UO_2, Ω_g is the Van der Waals volume of noble gases, Y is the yield of stable gases per fission, t is the total irradiation time, and D is diffusion coefficient. The bubble concentration is given by $C_B = \frac{\alpha}{\pi r_f R^2}$, where α

is the number of bubbles nucleated by fission (~5-20). In case the number of gas atoms in the bubbles is not small, the concentration C_B is replaced by $C = YFt$, where F is the fission density. The effective diffusion coefficient can then be related to the lattice diffusion D as follows:

$$D_s = \frac{2\pi F r_f R^2 D}{2\pi r_f R^2 + 4\pi D R C_B}$$

In this equation, $2\pi r_f R^2$ represents the probability of re-solution of a gas atom, and $4\pi D R C_B$ represents the probability of a gas atom capture at a bubble. In order to calculate the effective diffusion coefficient as a function of time, the aforementioned bubble radius equation can be substituted in. Then, the value of D_S is calculated for different α values (5, 10, and 20), and the results are compared to experimental values obtained from single crystals. Results show that at the beginning of the nucleation process of bubbles, a high amount of gas is present in the bubbles, and the effective diffusion coefficient is lower than the lattice diffusion coefficient. But, at longer times, the concentration of gas atoms in the bubbles starts to increase at slower pace than that of the gas atoms in the solution, and the effective diffusion coefficient approaches the lattice diffusion, which is in accordance with experimental observations.

As for the temperature dependence of the release process, it is apparent in Figure 2.6 that the diffusion coefficient does not depend on temperature if it is below 800 ℃, but the process becomes thermally activated at 800-1400 ℃, which is in agreement with a previous experiment done by Friskney *et al.* [25] as shown in Figure 2.6. Turnbull then affirms that the process of gas release is controlled by diffusion for temperatures ranging from 225 ℃ to 1400 ℃, and makes a comparison with a study done by Matzke [26], in which he investigates in-pile self-diffusion of cations for temperatures between 130 ℃ and 1500 ℃. Both studies agree that diffusion is athermal below 1000 ℃, and the radiation enhancement is due to fission fragments, where Matzke notes that α-bombardment using a Pu-238 sample do not show significant diffusion, even at high doses of α. The studies also agree that the diffusion coefficient is proportional to fission rate, and that the diffusion process shows signs of becoming thermally activated above 1000 ℃. Finally, Turnbull concludes that diffusion calculations should be divided into three temperature regimes; one for high temperatures for intrinsic diffusion, and two for radiation enhanced diffusion at lower temperatures. These diffusivity regimes are illustrated in Figure 2.7.

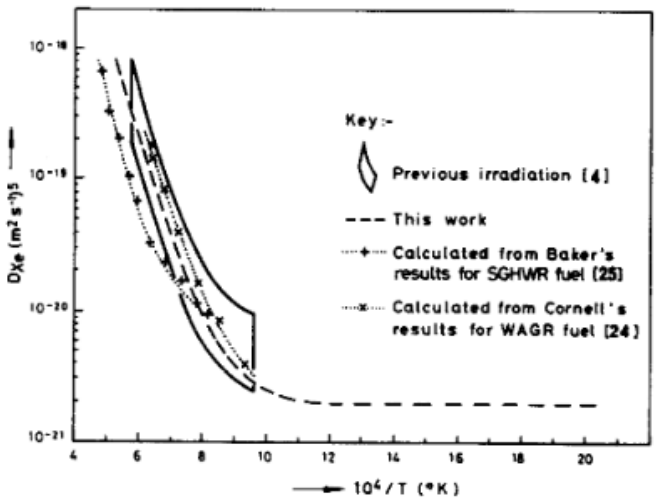


Figure 2.6: Xenon diffusion coefficient values from multiple sources, as reproduced from Ref. [13].

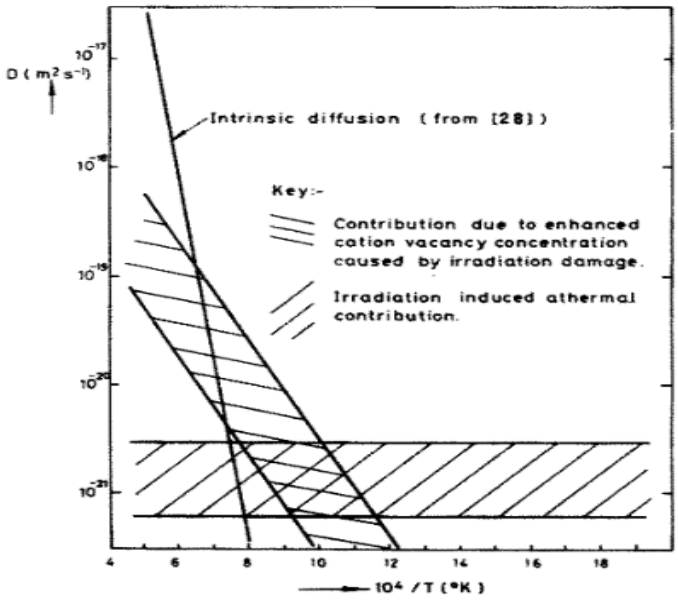


Figure 2.7: In-pile diffusion coefficients depending on temperature, as reproduced from Ref. [13].

In a recent study done by Setyawan [10], the heterogeneous re-solution rate was investigated. This re-solution mechanism depends on effective stopping power, bubble radius, and off-centered distance. Investigation of homogenous re-solution by looking at studies done by

Schwen [34] and Govers [23] confirm that homogeneous re-solution is insufficient (only 2-3 atoms dissolve from bubbles) to account for the empirical value that is fitted by Losonen [14]. The paper also mentions Huang's simulation to study the effect of effective electronic stopping power for tangential and on-centered geometries [11], and discusses a study by Govers [23], where the effective stopping power was specified as a parameter, but the study only shows results for on-centered geometries. While investigating on-centered thermal spike approach, Setyawan *et al*. discover that the fraction of re-solved gas atoms is independent of gas density in the bubble. Also, the larger the bubble the lower the re-solution rate, because gas atoms in the center of the bubble have a lower chance of dissolving out of the bubble. Therefore, higher thermal spike energies are needed to fully resolve large bubbles. The critical effective stopping power is discussed and is determined—for effective stopping power values below 9.04 KeV/nm, no re-solution occurs. Off-centered (tangential) geometry is then investigated, and it is confirmed that the fraction of re-solved atoms becomes zero at a critical off-centered distance r_c. Finally, an investigation of fission product yields and their kinetic energy was performed in order to finalize the re-solution equation. The mass of the most probable isotope is considered the atomic mass in order to simplify the calculation of the effective electronic stopping power. Only a percentage of the effective electronic stopping power is taken as thermal spike, and that is denoted by ζ. The values of re-solution rates based on zeta are evaluated in comparison to different studies done by Losonen, Turnbull, and Veschunov [14,4,20], and a value of 0.73 for ζ is considered a reasonable choice. The final heterogeneous re-solution rate equation is then given as:

$$b_{het} = 0.25\,\pi r_c^2 \dot{F} \sum_i y_i \int_{x=0}^{\mu_c, i} [1 - e^{-0.05(\zeta\, S_{e,i} - 9.04)/R^{1.47}}]dx$$

Where r_C is the off-centered distance between thermal spike axis and bubble center, $\dot{F}$ is the fission rate density, y_i is the independent fission product yield, $\zeta\, S_{e,i}$ is the effective electronic stopping power, and R is the bubble radius.

CHAPTER THREE

METHODS AND MODELING

3.1 Model Setup

In order to model the fission gas behavior in nuclear fuel, multiple scales must be considered. From the nano-scale of fission gas formation and bubble nucleation to the centimeter-scale of the fuel pellets, a meso-scale model is to be constructed to capture all stages that lead to fission gas release. And since these three stages happen at different irradiation times, noting that they can occur simultaneously, the model must also be multi-time scaled. This helps in obtaining more accurate results with lower uncertainties. Powerful computational tools are used to simulate at least a few hundred particles in order to get less biased results and more reliable data. The Xolotl-fission code is used in this research to describe the evolution of intra-granular bubbles. The gas re-solution from bubbles back to the fuel has been recently implemented in the code, which provides a better understanding of the true mechanisms of fission gas behavior with less uncertainty, unlike previous models. Future work also includes performing uncertainty quantification analyses on Xe gas behavior in nuclear fuel, and to be able to describe the inter-granular bubble evolution as well. MD simulations are used to determine the diffusivities at intrinsic, irradiation enhanced, and athermal diffusion conditions. Since the vacancy migration is what dominates the bubble formation and growth, the process is relatively slow, and thus AMD simulations are needed to accelerate the process of finding these diffusivities.

3.2 General Information and Current State of Xolotl

Xolotl is the simulator used to produce the results presented in this thesis. The name comes from Aztec mythology—pronounced as SHO-lottle, referring to the god of fire, lightning, and death. It is a cluster dynamics simulator written in C++ and is used to predict and visualize the behavior of bubbles in solids, the solid being UO_2 [uranium dioxide] in this research. When using Xolotl, the Message Passing Interface (MPI) is employed in order to achieve parallel computing. When it comes to visually analyzing the results obtained using Xolotl, EAVL is the library of choice. This library provides the capability of viewing results in 1D, 2D, or 3D depending on the context of the data set in question. Xolotl is also built around PETSc (PET-

see), which is a solver library used to solve models that are constructed by partial differential equations (Blondel *et al.* [31]).

In this project, the powerful computational capabilities of the University of Tennessee, Knoxville Advanced Computing Facility (ACF) has been utilized to run Xolotl. This shortens the running time of the simulation tremendously—simulations that could take weeks on a personal computer, take a few minutes when they are ran on ACF. The process of running Xolotl on ACF is simple, once it is installed. First, a file with specified parameters is written. Then, a script is constructed in order to submit the desired job to ACF. The number of nodes used to run the job can be specified in this script, along with the preferred name of the output files and the preferred location to store them. Finally, this job script is initiated using the "qsub" command in a computer terminal. The script must have ".qsub" as its extension, in order for the job to be initiated on ACF. Currently, the resulting output files include a log file to show the date and time of the job's initiation, the material used, and the concentration at each time step; a file documenting the resulting average radius and re-solution rate at each time step; HDF5 file; and finally an error file in case of incorrect parameter input.

3.3 Xolotl Input Parameters and Output Files

There are many parameters that Xolotl uses as input. This section briefly explains each of the parameters used in this research. The parameters and a brief description are shown in the Table 2. Some of the mentioned parameters should not be used together. For instance, only one of two options is needed when it comes to selecting the temperature—either "tempFile" or "startTemp." Another example is using the "networkFile" option. That option selects an HDF5 file to act as an initializer of the simulation. When that is done, the simulation will take on the "grid" and "netParam" input values of the previous simulation that resulted in the selected HDF5 file, and thus the latter two options should be removed from the input file of the new simulation. This option is of tremendous help when running sequential simulations, where the process of running each subsequent simulation can be automated with a properly written job script.

Xolotl can also be used in other cases dealing with helium irradiation and Tungsten. Input parameters relating to those cases, and more extensive description of the already mentioned parameters, can be found on the github website under the Xolotl wiki page [16].

Table 2: A table describing some of the input parameters of Xolotl, as reproduced from Ref. [16]

petscArgs	The parameter needed to modify PETSc options (e.g. maximum run time and number of time steps)
vizHandler	The visualization handler used (std,dummy)
flux	Fission rate density [fissions/nm^3/s]
netParam	5 integers: size values of the largest cluster (Xe or He), largest D cluster, largest T cluster, largest vacancy, and largest interstitial
material	The material used. Tungsten (irradiated by 200 eV He) and UO_2(irradiated by Xe)
dimensions	The number of dimensions for the simulation (0-3)
perfHandler	Performance handlers (std, dummy, os, or papi)
tempFile	Temperature profile where the data is given through a linear interpolation
startTemp	The constant temperature in Kelvin. Adding a second temperature creates a gradient, where the first value is surface temperature and the second value is the bulk temperature
grouping	Grouping parameter where the first integer is the starting size and the second is the first width of the group
process	The physical process of the simulation (e.g. reaction and re-solution)
zeta	To select the fit that represents the percentage of electronic stopping power that is taken as thermal spike for re-solution
density	Value of the inverse atomic volume [Xe/ nm^3]
resoSize	Minimum bubble size for re-solution to occur
radiusSize	Sets the minimum size to compute the average radius
networkFile	The name of the HDF5 that acts as a starting point of the simulation

CHAPTER FOUR

RESULTS AND DISCUSSION

4.1 Sensitivity Analysis without Re-solution

In this section, the results of sensitivity analysis performed relying on data from literature are presented. First, the effects of time and temperature on bubble evolution are explored. The selection of temperatures is based on data from a study done by Cornell [6]. As seen in Figure 4.1, increasing the temperature results in a slight increase in the average radius. This is attributed to the increase in diffusion that happens when the temperature is increased, based on the previously discussed temperature regimes constructed and presented by Turnbull [13]. For instance, the diffusion coefficient when operating at 1560 ℃ is calculated to be 3.327 $\left[\frac{\mathrm{m}^2}{s}\right]$ using the appropriate equation for that temperature. On the other hand, the diffusion coefficient for 1000 ℃ is much smaller, with a value of $6.4 * 10^{-30}$ $\left[\frac{\mathrm{m}^2}{s}\right]$. Meaning that diffusion takes place more rapidly when operating at higher temperatures. On the other hand, the reason why time affects the average size of the bubble is that the gas atoms, namely Xe atoms, can travel for longer distances and get captured by bigger bubbles that act as a stronger sink.

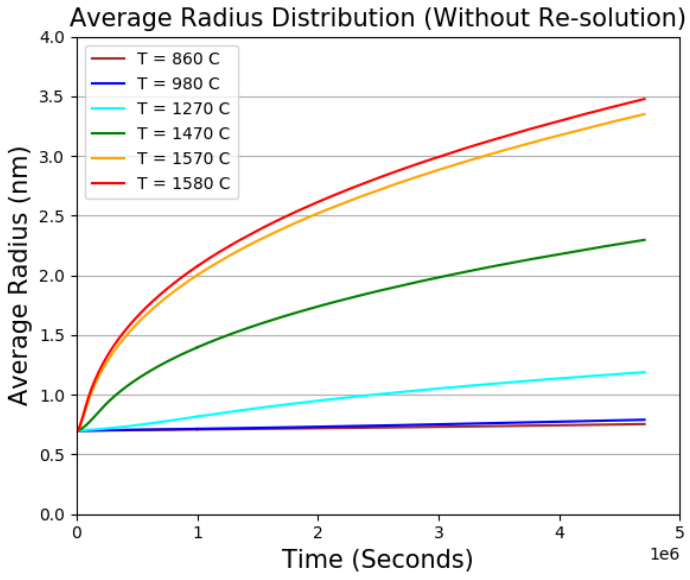


Figure 4.1: Plot of the average radius plotted against time of various temperatures selected based on Cornell *et al.* [6].

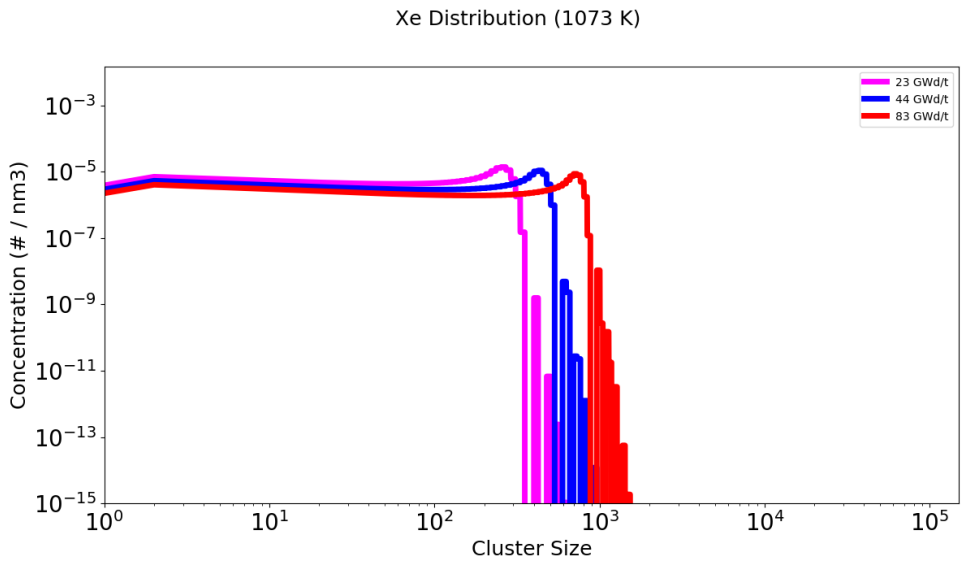


Figure 4.2: Xenon bubble distribution obtained by simulating a fission rate density of 8e18 fissions/nm3/s with operating temperature of 1073 K for 23, 44, and 83 GWd/t burnups.

In other words, the overall concentration of bubbles decreases over time, while the size of bubbles that were originally large experiences a further increase. This can be seen in Figure 4.2.

4.2 Effects of Implementing Re-solution

As discussed in the background section, the heterogeneous re-solution rate devised by Setyawan et al. [10] is dependent upon effective electronic stopping power, bubble radius, and off-centered distance. This rate is implemented in Xolotl, and its values are compared to the results from the paper in Figure 4.3 for different Z values (denoted ζ in the paper) and starting at 0.3 nm radius in Xolotl. As seen in the figure, increasing the thermal spike increases the re-solution rate. Results from Xolotl are identical to results from [10], which means the re-solution rate has been implemented correctly in Xolotl. In order to investigate the effects of re-solution on bubble evolution behavior, a simulation was performed using different Z values and plotted in Figure 4.4. The plot represents the bubble evolution in terms of cluster size (measured in terms of the number of xenon atoms in a bubble) and the concentration of bubbles (number of bubbles per nanometer cubed). Increasing the percentage of stopping power that is counted as thermal

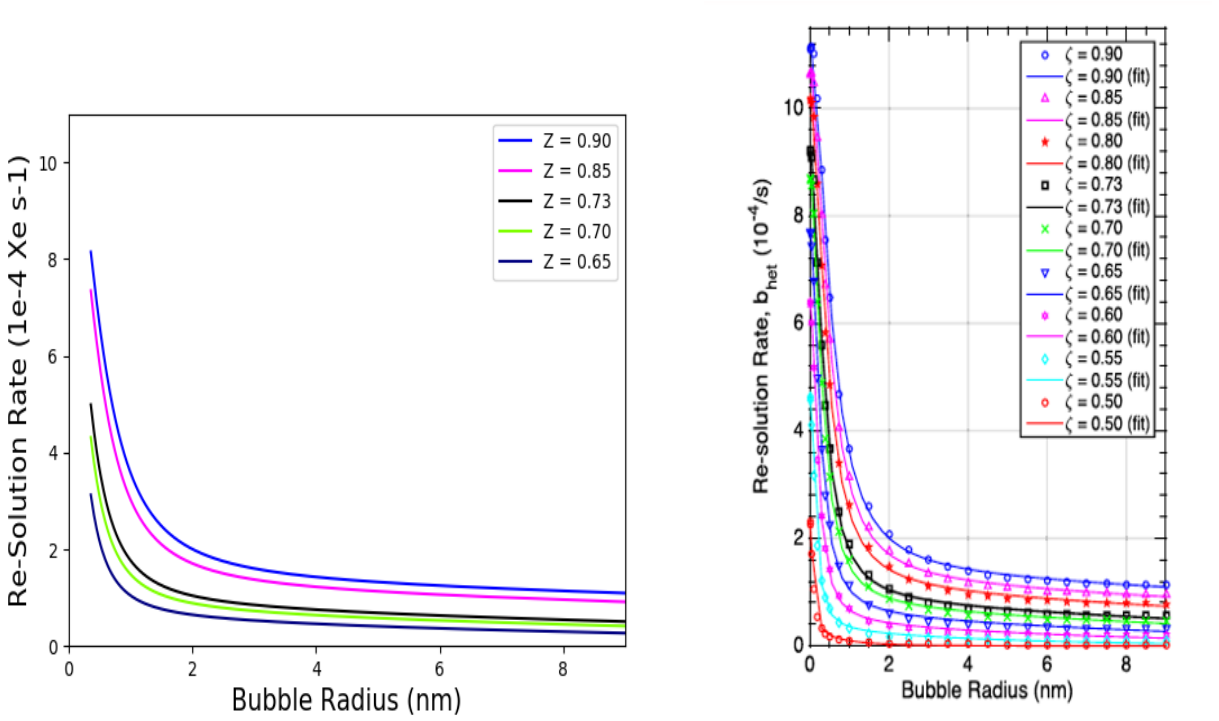


Figure 4.3: Heterogeneous re-solution rate as a function of the percentage of effective electronic stopping power taken as thermal spike. Xolotl results appear on the left, while the right plot is from Setyawan [10].

spike results in increasing the re-solution rate. This leads to more xenon atoms getting "knocked out" of the smaller sized bubbles, which decreases their concentrations. These xenon atoms diffused and are absorbed by the bigger bubbles. As can be seen in Figure 4.4, the highest cluster size is reached when using the highest Z value, because that is the highest re-solution achieved in this simulation. Also, as seen in Fig 4.3, the re-solution is less effective for larger bubbles. Another way to test the effect of Z value on the bubble evolution is to test its effects on the average radius of bubbles over time. In this simulation, the average radius is calculated only for bubbles with a radius larger than 1 nm. Results are plotted and shown in Figure 4.5. The results show that the average radius increases as Z is increased, for the same reasons mentioned for Figure 4.4.

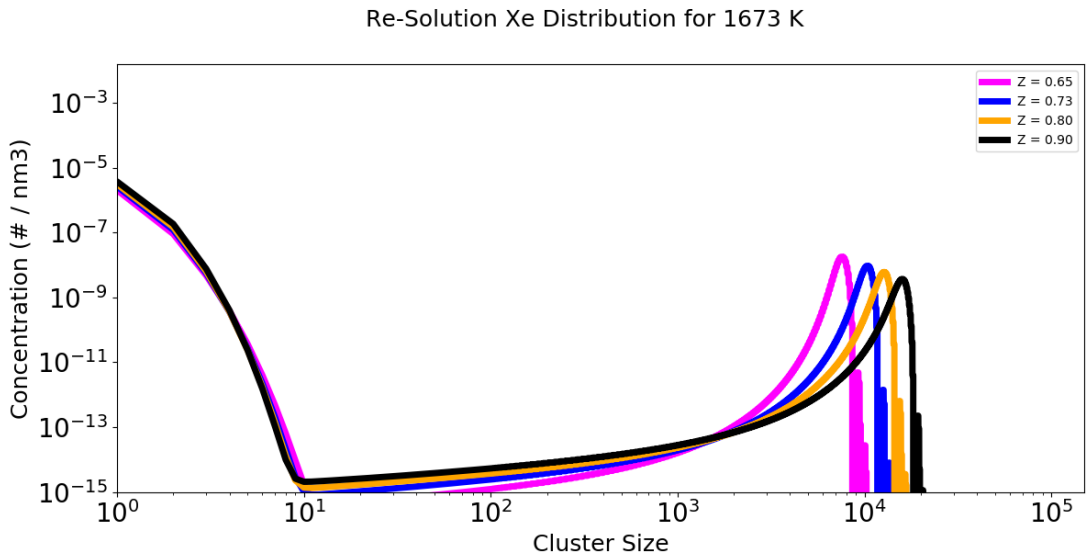


Figure 4.4: Xe bubble size distribution for different values of thermal spike.

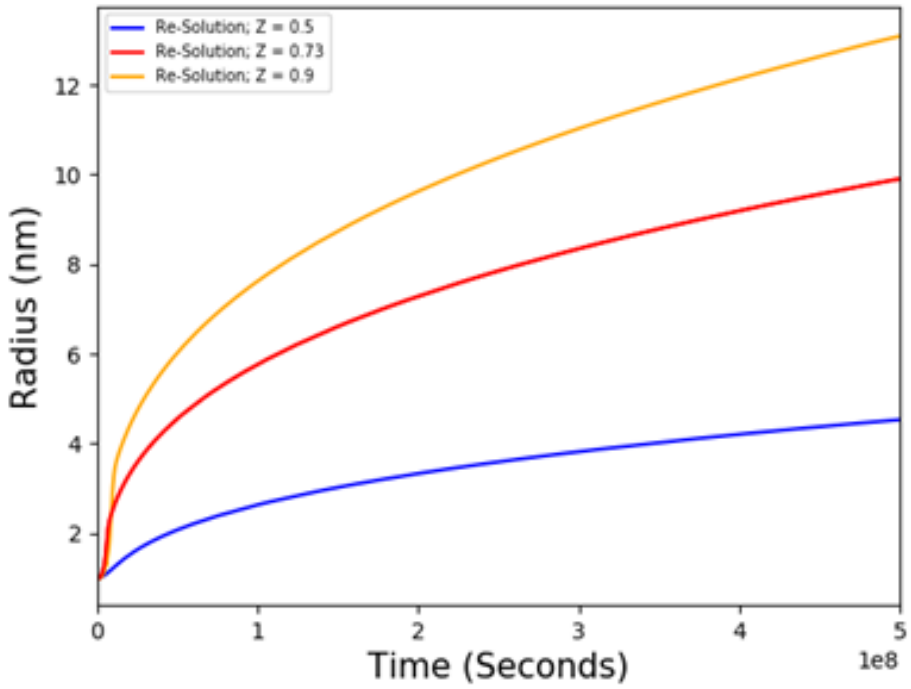


Figure 4.5: A plot showing the effects of increasing the of stopping power that is taken as thermal spike Z on the average radius over time. The average radius is only calculated for bubbles that are larger than 1 nm.

Another important parameter is the reaction radius (R), which is dependent on the inverse of the atomic volume of xenon, and the number of xenon atoms in a bubble. This is shown in the equation below:

$$R = \left(\frac{3 * N}{4 * \pi * \rho}\right)^{\frac{1}{3}}$$

Where N is the number of xenon atoms in bubbles and ρ is the atomic density (Xe/nm^3), which results in a value of R in nanometers. The values of the reaction radius (R) used in this research are taken from Setyawan *et al.* [10], and the effect of varying this parameter is shown in Figure 4.6. As seen in Figure 4.6, changing the reaction radius has a very small, almost negligible effect on re-solution rate, as suggested by Setyawan. Therefore, the value of 10.5 $[\frac{Xe}{nm^3}]$ is selected for the remainder of the simulations presented in this thesis.

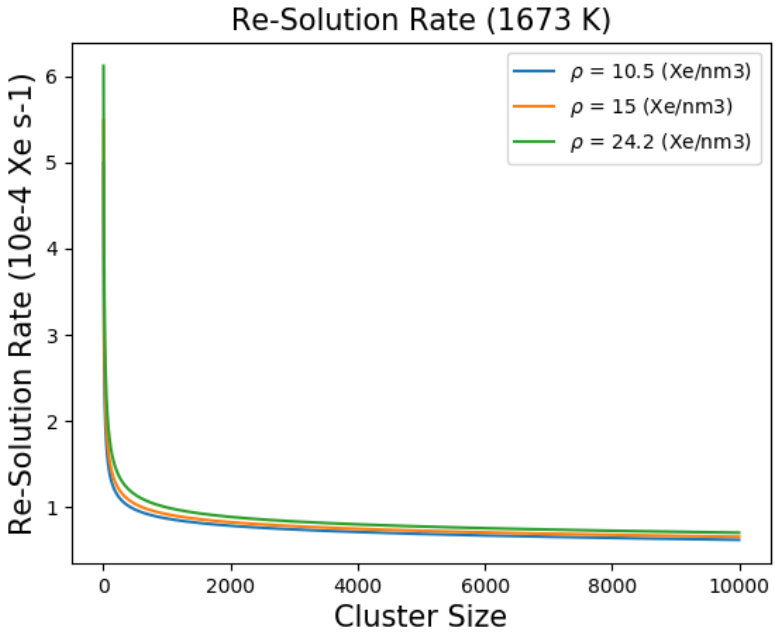


Figure 4.6: Plot showing the effects of varying the reaction radius on re-solution rate.

4.3 Sensitivity Analysis with Re-solution

After the implementation of re-solution, sensitivity analysis is performed based on data from Cornell and Baker [6,7]. The first simulation is done based on Cornell's data, where a burnup of $3.2 * 10^{25} \frac{fissions}{m^3}$ is used, in order to compare the bubble radius and number density while varying temperature. Table 3 shows results from Cornell, as opposed to results obtained from Xolotl. As mentioned in the background section, the radius measured by Cornell is incorrect, and an appropriate correction is shown in the Table 3. The results that are obtained using Xolotl show an overestimation of bubble radius, and a clear underestimation of bubble number density. A visual representation of Xolotl results can be seen in Figure 4.7.

Table 3: Comparison of bubble radius and number density between Cornell [6] and results obtained using Xolotl

Temperature (°C)	**Bubble Radius (nm)**	**Bubble n.d. (m^{-3})**	**Corrected Radius (nm) (Reduced by 35%)**	**Xolotl Radius (nm)**	**Xolotl n.d. (m^{-3})**
860	0.85	$3.80 * 10^{23}$	0.55	1.81	$2.50 * 10^{22}$
980	0.9	$3.50 * 10^{23}$	0.58	1.93	$2.28 * 10^{22}$
1270	1.00	$2.90 * 10^{23}$	0.65	2.17	$1.72 * 10^{22}$
1470	1.15	$1.83 * 10^{23}$	0.75	2.63	$9.90 * 10^{21}$
1570	1.30	$1.24 * 10^{23}$	0.84	3.43	$4.50 * 10^{21}$
1580	1.40	$1.18 * 10^{23}$	0.91	3.55	$4.09 * 10^{21}$

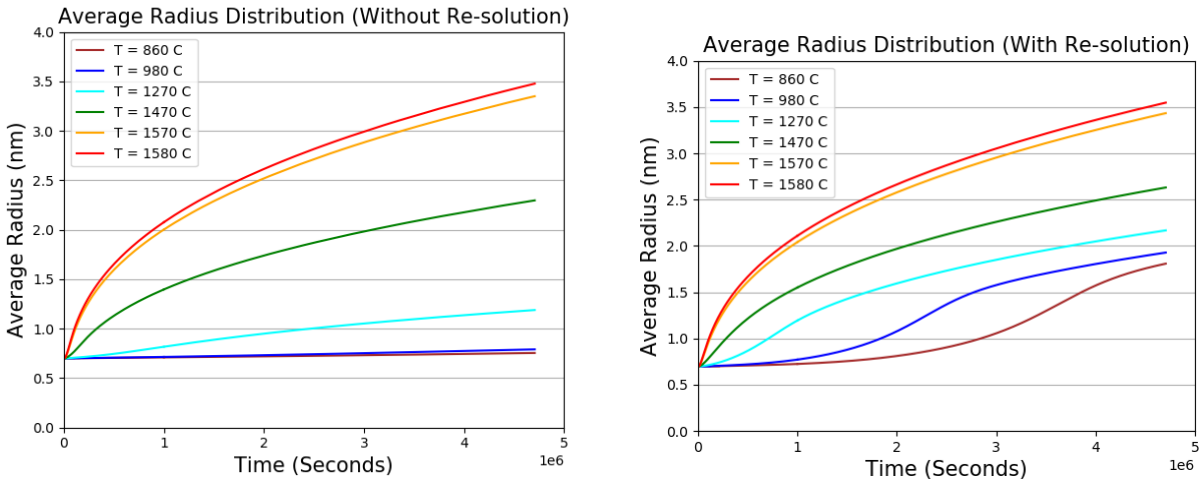


Figure 4.7: Average radius of bubbles with radius bigger than 0.7 nm at different temperatures with and without re-solution. The plots are generated from results obtained through Xolotl, based on parameters taken from Cornell [6].

As previously discussed, the re-solution affects smaller bubbles more than it affects larger bubbles, which is shown in Figure 4.7. It is more difficult to knock out gas atoms that are placed in the center of a bigger bubble. Also, bigger bubbles have more chance to absorb gas atoms that are not in bubbles, so they act like a stronger sink than smaller bubbles.

4.4 Bimodal Distribution

As discussed in the literature review, the behavior of the bubble evolution exhibits a tendency to form a bimodal-shaped, or sometimes multi-modal, distribution—referring to the number of prominent, well defined peaks which represent the number of bubbles that have two or more different sizes. Efforts have been made during this research to first test the ability of Xolotl to produce results exhibiting a bimodal distribution, then testing whether the bimodal distribution persists or disappears after using an artificial distribution is created to start the simulation. The process of this test is simple, yet important. First, a bimodal distribution is artificially created where there is a high concentration of bubbles containing 200 xenon atoms and bubbles containing 3000 xenon atoms at 0 seconds. That network file is then used to start another simulation, where the bubbles are allowed to evolve without constraints. The first

simulation is run for $1.5 * 10^8$ seconds, and the results are presented in the Figure 4.8. Re-solution is on during this simulation, and the reaction radius and Z values are 10.5 Xe/nm^3 and 0.73 respectively. The results show that bimodal distribution somewhat persist, but the first peak is not prominent. This is due to the fact that re-solution has less of an effect on larger bubbles because it is more difficult to knock-out the xenon atoms at the center of the larger bubbles. Also, the larger bubbles act as a stronger sink for single xenon atoms to be absorbed and further increase the size of those large bubbles.

A second test is then conducted where the simulation starts with an artificially created bimodal distribution, and another simulation is done for 5e7 seconds with re-solution turned off for one set of data, and on for another (Figure 4.9).

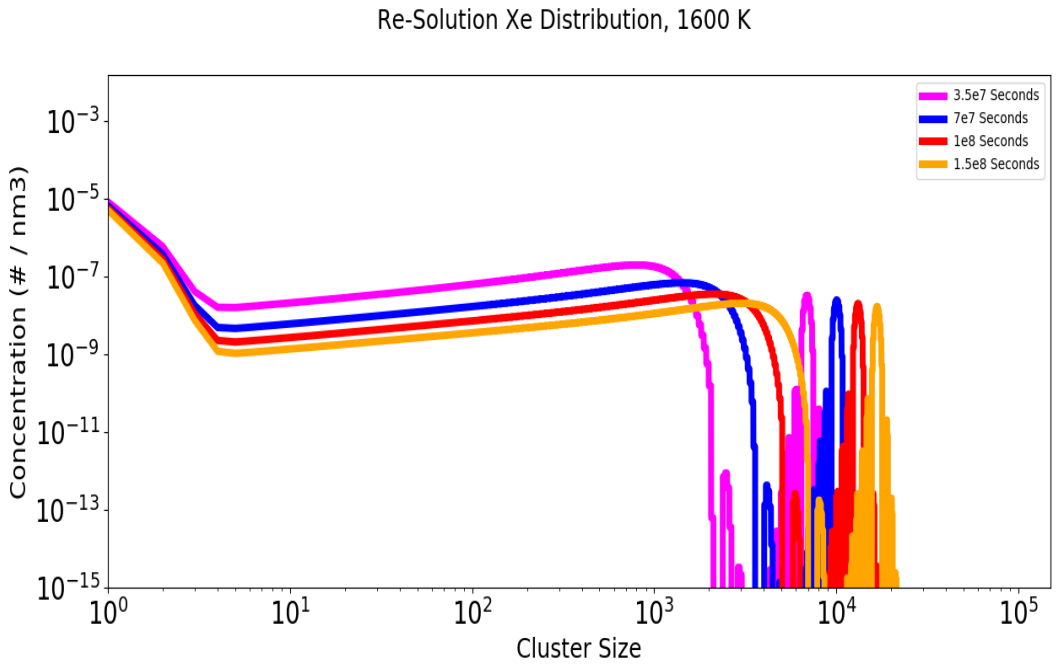


Figure 4.8: Xe bubble distribution after using an artificially created bimodal distribution with concentration peaks at 200 and 3000 Xe atoms. For temperature of 1600 K and fission rate density of $8 * 10^{18} \frac{fissions}{m^3 * second}$

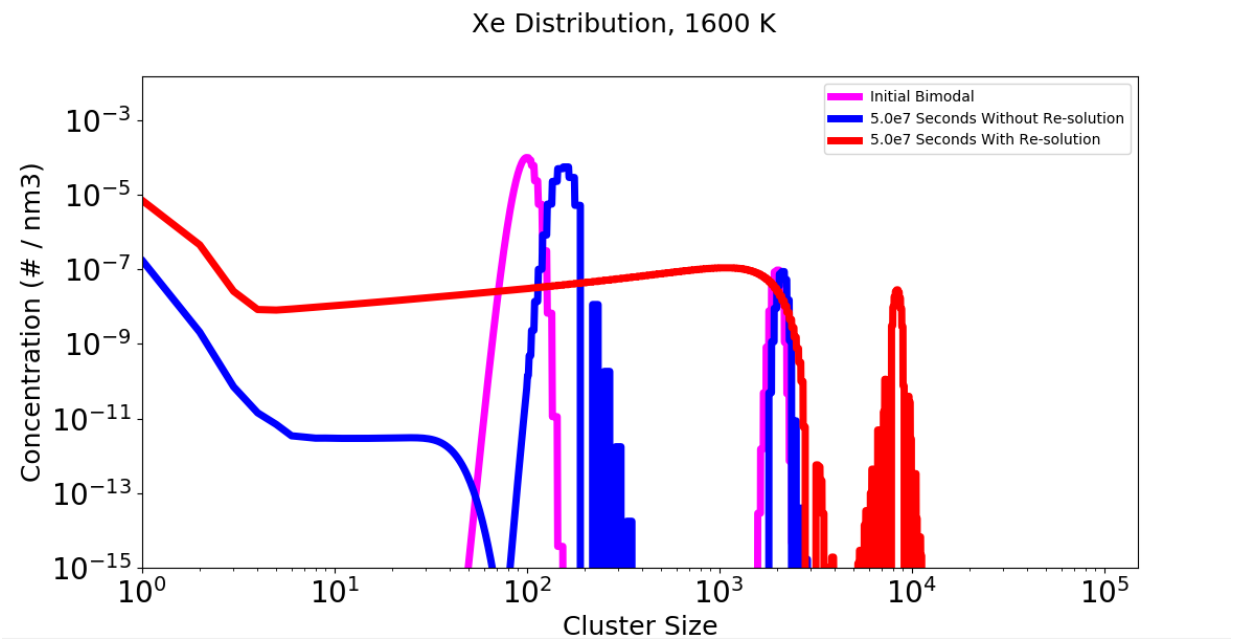


Figure 4.9: Xenon distribution after starting with an artificially created bimodal shape. The initial bimodal shape is shown in magenta color, followed by two separate simulations—the first simulation is done without re-solution (shown in blue), and the second is done with re-solution (shown in red).

The results show that the bimodal distribution persists in a more prominent manner when the re-solution is turned off.

In order to confirm this observation, other tests were conducted. One involved a simulation without an artificially created bimodal distribution. Starting with re-solution, and using the resulting network file to start another simulation with the re-solution turned off. The results are presented in the figure below. This clearly shows two prominent peaks at different cluster sizes, which means the bimodal size distribution is exhibited when a simulation starts with re-solution and then the re-solution is turned off. Although this process is not physical, it gives further perspective about the bubble behavior and how the bimodal distribution can in fact persist in Xolotl.

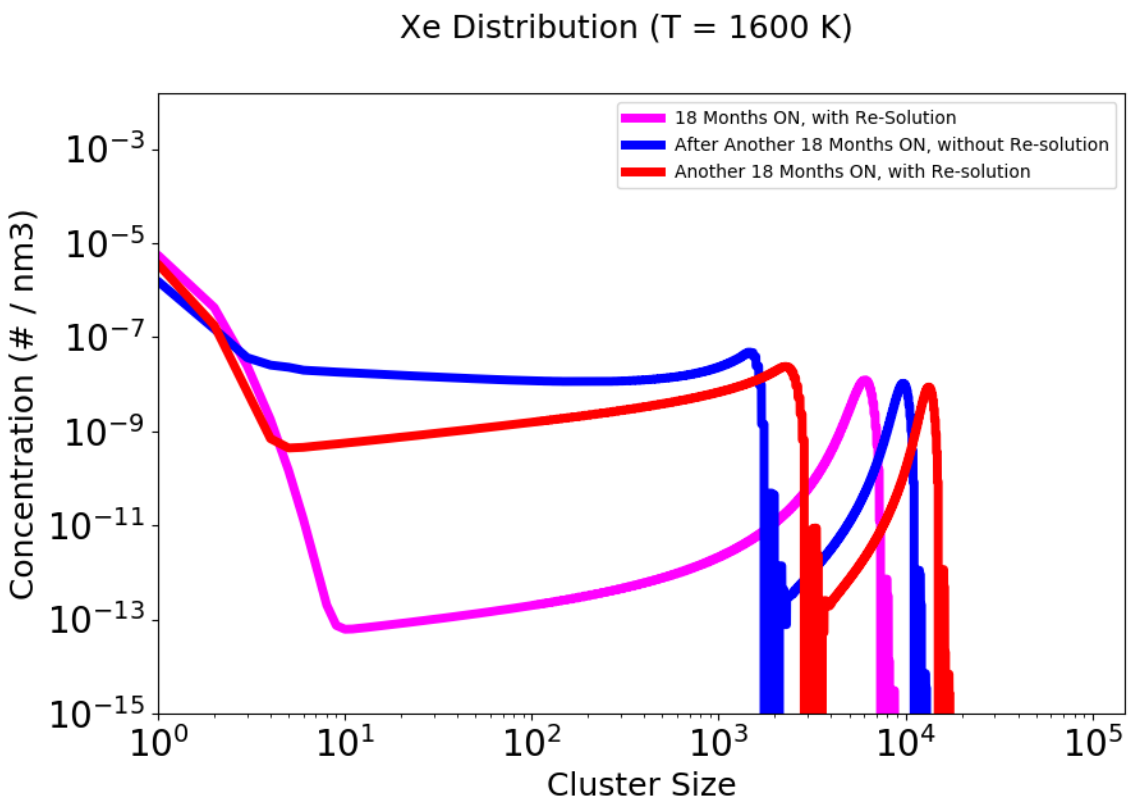


Figure 4.10: Xenon distribution as a result of varying re-solution. Starting a simulation with re-solution (magenta curve), then turning the re-solution off (blue curve) for 18 months but keeping the same fission rate density, then turning the re-solution back on (red curve).

4.5 Diffusion Coefficient

Another parameter that is investigated in this research is the effects of varying the diffusion coefficient beyond Turnbull's model [13]. As discussed in the background section, Turnbull came up with a model to divide the diffusion coefficient calculations into three regimes depending on the operating temperature. The first regime is the intrinsic diffusion regime, at high operating temperatures (1650 K > T). The second regime considers radiation enhancement of diffusion at intermediate temperatures (1381 < T < 1650 K). Finally, the third regime where the diffusion coefficient is unaffected by temperature and is only affected by the fission rate at low operating temperatures (T < 1381 K). That being said, it is of interest to calculate the diffusion coefficients using Turnbull's equations with no regard to the temperature ranges he suggested.

This is done to see the effect of increasing the diffusion coefficient at lower temperatures without increasing the fission rate, and the resulting fission gas behavior, using Xolotl.

The first test is conducted using the suggested temperature regimes for reference. It is a multi-step test, where the simulation starts with an operating temperature of 1573 K, fission rate density of 8e18 ($fissions/m^3/s$), Z value of 0.73, and an inverse atomic volume of 10.5 (Xe/nm^3). The simulation runs for 18 months using the mentioned parameters. The results of this simulation are then used as a starting point for a second simulation, where all the parameters are kept the same except for the temperature which is decreased to 600 K, and the fission rate is zero. The second simulation then runs for one month. The reason for turning the fission rate off and decreasing the temperature is to simulate the fission gas behavior in the fuel when the reactor is turned off. In the third step, the reactor is turned back on—meaning the temperature is increased back to 1573 K, and the fission rate density is turned back on with the value of 8e18 (fissions/m3/s). As previously mentioned, the calculated diffusion coefficient for each step is done by employing Turnbull's equations at the suggested temperature ranges. The same test is then conducted again, but with different diffusion coefficients—this time, the radiation enhanced diffusion coefficient (D from the second regime) is used for the shutdown phase of the reactor. All of these tests are done twice, once with re-solution turned on and once with re-solution turned off. The results are then plotted and compared, as can be seen below.

The results show that increasing the diffusion coefficient leads to a decrease in the monomer concentration and shows a bimodal distribution in Figure 4.11 c) and d) where the diffusion coefficients are highest when the reactor is off. However, the bimodal shape does not persist. This could be attributed to the fact that the first concentration peak is happening at very small bubble sizes (~ 0.6 nm radius bubbles), and when re-solution is turned back on, these small bubbles are easily destroyed.

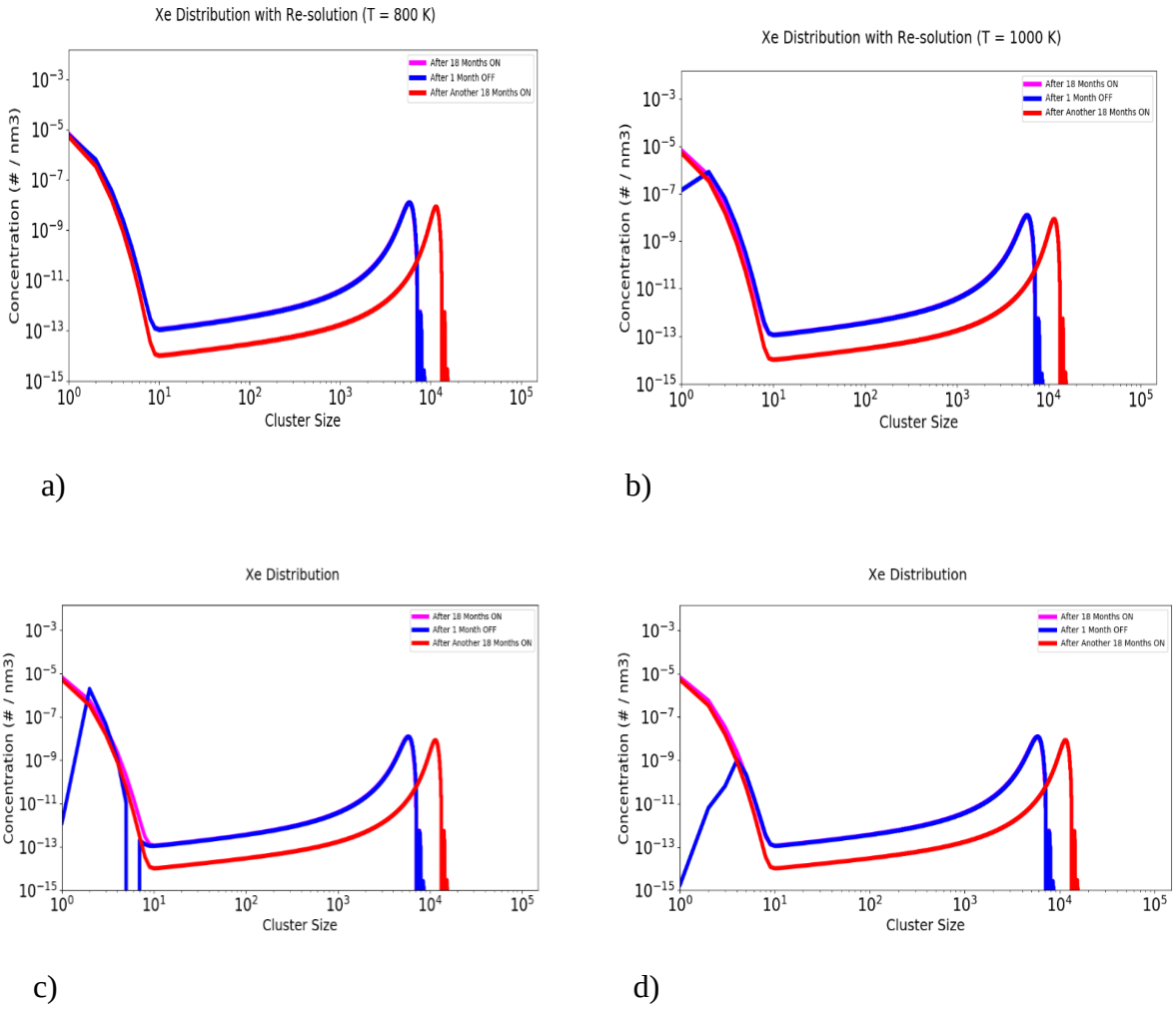


Figure 4.11: Effects of diffusion on the size distribution for different temperatures. a) Represents the plot for 800 K with diffusion coefficient of 4.363e-5 nm^2/s using Turnbull equation from regime 2 (radiation enhanced). b) Represents 1000 K with diffusion coefficient of 1.418e-3 nm^2/s using Turnbull equation 2 also. For c) and d) the diffusion coefficients are multiplied by 10^6, and the values are 43.63 nm^2/s and 1418 nm^2/s, respectively.

4.6 Annealing

The last part of the simulations performed using Xolotl during the time of this research is related to the annealing experiments conducted by Kashibe et al [8]. The method and parameters used in Xolotl to replicate those annealing experiments are the following: in the beginning, the reactor is on, meaning that there is fission rate which is selected to be $8\,x\,10^{18}\,m^{-3}s^{-1}$ [fissions per meter-cubed per second]. The starting temperature is 1073 K, and the simulation stops at a burnup value of 23 GWd/t [Giga-Watt-Day per ton]. Then, the reactor is turned off (the fission rate is now zero, and there is no re-solution), and the temperature is increased to 2073 K with a rate of 1.7 C/s (Celsius per second) and is held for five hours. After that, the temperature is immediately cooled down to room temperature levels (293 K). In this test, the re-solution is off throughout all simulations. However, a second test is conducted with the same parameters and method, except the re-solution is turned on during the first phase only (until reaching 23 GWd/t burnup). Four more tests are conducted afterwards, for burnup values of 44 and 83 GWd/t. The results are presented below, in figures 4.12-4.14.

As observed in Figure 4.12, the concentration of the monomers decreases after the annealing process. Also, more xenon atoms get trapped in bigger bubbles (the number density of bubbles containing 100 xenon atoms increases). However, when compared to results obtained by Kashibe et al [8], the first peak happens at a much smaller size than what they observed. This trend persists for higher burnups, and as the burnup increases, the bubble size also increases. This can be seen in figures 4.13 and 4.14. Although results from Xolotl show an increase in bubble size with increasing burnup, the annealing effects found in the Kashibe experiment are not achieved in Xolotl. After annealing, Kashibe found that the bubbles reach tremendously large bubbles of ~800 nm. However, the largest size resulting in Xolotl is on the order of 22 nm. This discrepancy can be attributed to the fact that Xolotl does not include a vacancy absorption mechanism, nor does it include a bubble coalescence mechanism.

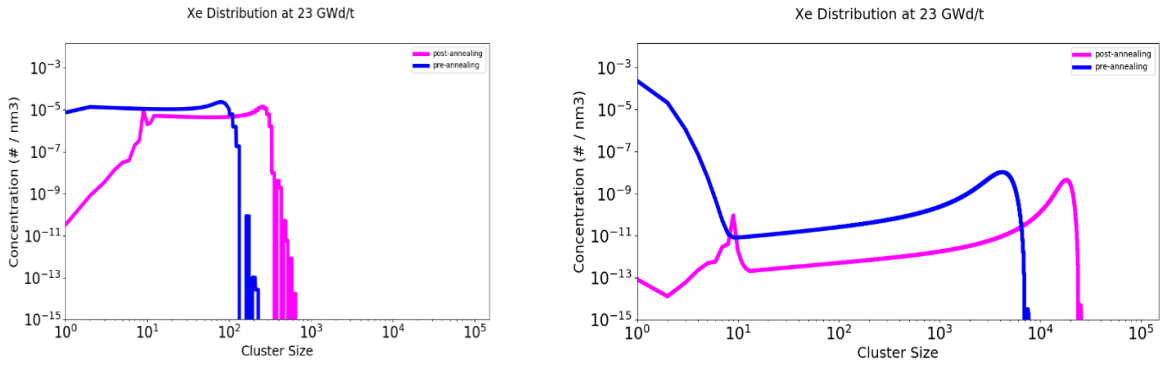


Figure 4.12: Xolotl plots of Xe distribution based on Kashibe experiment [8] where a sample is irradiated to 23 GWd/t. The sample is then annealed at a temperature of 2073 K for five hours, then the samples are immediately cooled down to room temperature. The results are shown without re-solution (left) and with re-solution turned on (right).

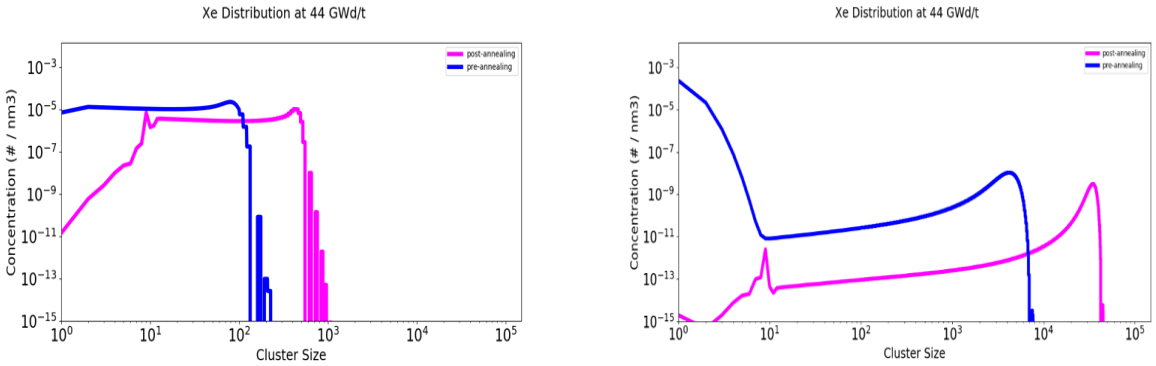


Figure 4.13: Xolotl plots based on Kashibe experiment [8] where a sample is irradiated to 44 GWd/t. The sample is then annealed at a temperature of 2073 K for five hours, then the samples are immediately cooled down to room temperature. The results are shown without re-solution (left) and with re-solution turned on (right).

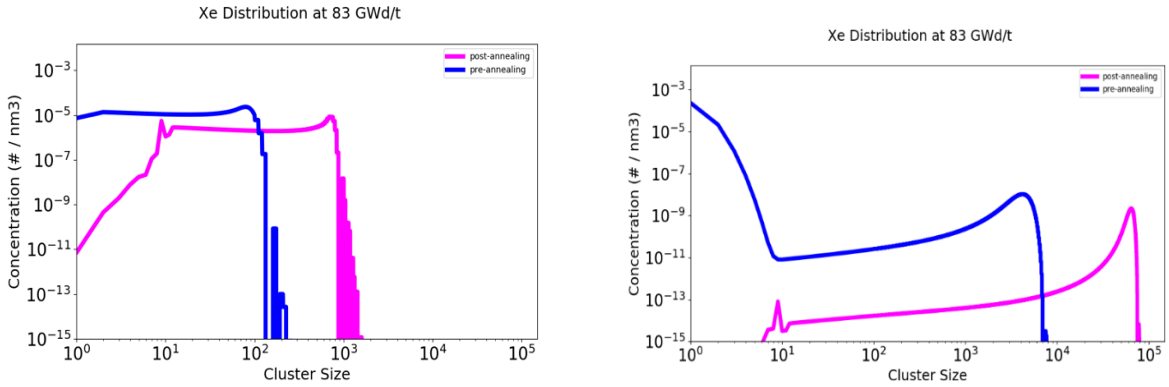


Figure 4.14: Xolotl plots based on Kashibe experiment [8] where a sample is irradiated to 83 GWd/t. The sample is then annealed at a temperature of 2073 K for five hours, then the samples are immediately cooled down to room temperature. The results are shown without re-solution (left) and with re-solution turned on (right).

A follow-up test is carried out using Xolotl, where annealing takes place after reaching a burnup of 23 GWd/t. The same method is used as the previous tests in this section, with the following exceptions. In this test, annealing takes place once, and the results are used as a starting point to reach 44 and 83 GWd/t burnups, while disregarding the cooling phase. Meaning, the reactor is on with 1073 K operating temperature and $8\ x\ 10^{18} fissions\ m^{-3}s^{-1}$ fission rate density, until reaching 23 GWd/t burnup. Then, the temperature is increased to 2073 K while the reactor is turned off—the fission rate density is now zero, and there is no re-solution. The "OFF phase" is held for 48 hours, then the reactor is turned back on until reaching 44 then 83 GWd/t burnup. The same test is done again, with re-solution turned on in the "ON phase" of the reactor until reaching 23 GWd/t burnup. As seen in figure 4.15, there is a second concentration peak of small bubbles after annealing. However, that peak flattens out when the reactor is turned back on. This could be due to the re-solution affects small bubbles a lot more than it affects larger bubbles. The peak after annealing is at bubbles with 0.7 nm size. Perhaps if that peak formed for bubbles with a larger size, the bimodal shape would have persisted.

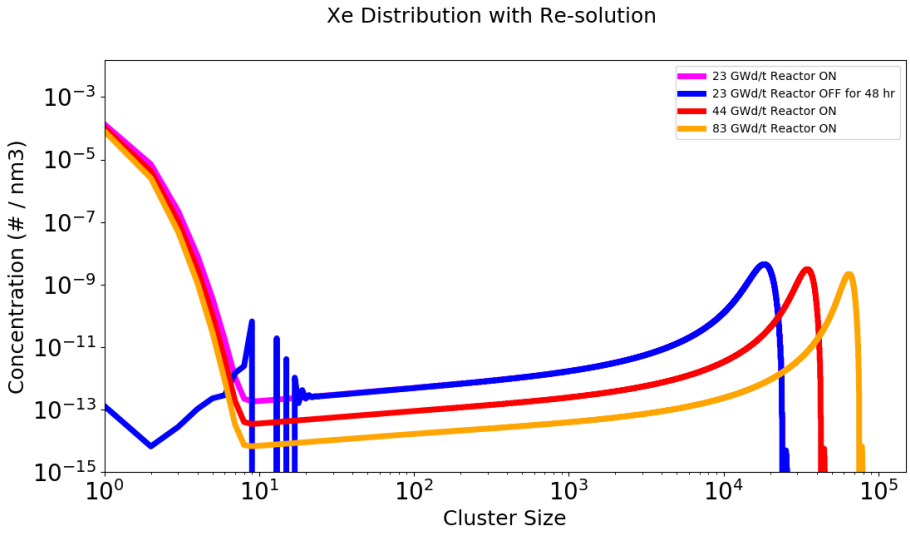


Figure 4.15: Annealing test results obtained using Xolotl. The reactor is turned on until reaching 23 GWd/t burnup (magenta curve). The reactor is then turned off and the sample is annealed (blue curve). Finally, the reactor is turned back on until reaching 44 and 83 GWd/t, depicted as red and yellow curves, respectively.

CHAPTER FIVE

SUMMARY AND CONCLUSIONS

A comprehensive model is required to assess the behavior of fission gas bubbles in nuclear fuel before gas release into the free volume of the fuel rod. Before the gas escape, there are three stages that take place in the fuel. Starting with fission gas diffusion and trapping by intra-granular bubbles; followed by nucleation, growth, and interconnection of inter-granular bubbles; and finally the escape/release of fission gas through the interconnected grain boundaries. The focus of this research is the first stage—the behavior of intra-granular bubbles.

Results show that the average radius is overestimated in Xolotl, while the bubble number density is greatly underestimated. On the other hand, Xolotl results show agreement when it comes to the largest bubble sizes formed, especially when compared to Kashibe. However, the average radius is still overestimated, and a prominent bimodal shape is not present. Also, the bubble size that are reached in Kashibe are not seen in Xolotl. This is attributed to the fact that Xolotl does not include a coalescence mechanism, nor does it include a vacancy absorption mechanism. These two mechanisms must be added in order to give an accurate representation of what happens at very high temperatures during annealing. The focus should be the vacancy absorption mechanism, because it does not only occur during annealing—there are vacancies produced due to fission fragments. Also, bubble motion is highly unlikely, as explained by Cornell, Baker, and Kashibe, and thus it hinders intra-granular bubble coalescence.

It is also important to investigate stoichiometric effects on xenon migration. A study by Catlow [27] deduces that noble gas atoms can occupy sites that have been vacated by anion and cation clusters, as mentioned by Turnbull [13]. And since the migration of a xenon-vacancy cluster is a slow process, it makes the intra-granular bubble formation and nucleation the limiting step for the entire process of fission gas release to the plenum.

LIST OF REFERENCES

1- Olander, and D.R. “Fundamental Aspects of Nuclear Reactor Fuel Elements.” Fundamental Aspects of Nuclear Reactor Fuel Elements (Technical Report) | OSTI.GOV, 1 Jan. 1976.

2- B. Smith, G. Pastori, D. Andersson, D. Bernholdt, H. Najim, and B. Wirth *et al.* “Advancing Understanding of Fission Gas Behavior in Nuclear Fuel through High Performance Computing.” https://nsuf.inl.gov/documents/Review2017/Andersson%20HPC%20Access.pdf

3- D. Andersson *et al*. “Atomistic Modeling of Intrinsic and Radiation-Enhanced Fission Gas (Xe) Diffusion in UO2±x: Implications for Nuclear Fuel Performance Modeling.” *Journal of Nuclear Materials*, North-Holland, 31 Mar. 2014, www.sciencedirect.com/science/article/pii/S0022311514001664.

4- Turnbull *et al.* “The Diffusion Coefficients of Gaseous and Volatile Species during the Irradiation of Uranium Dioxide.” *Journal of Nuclear Materials*, North-Holland, 26 Feb. 2003, www.sciencedirect.com/science/article/pii/0022311582904196?via=ihub.

5- Was, Gary S. “Fundamentals of Radiation Materials Science.” *Metals and Alloys | Gary S. Was | Springer*, Springer-Verlag Berlin Heidelberg, www.springer.com/us/book/9783540494720.

6- Cornell, Speight and Masters, Journal of Nuclear Materials 30 (1969) 170-178.

7- Baker, Journal of Nuclear Materials 66 (1977) 283-291.

8- S. Kashibe, K. Une and K. Nogita, “Formation and growth of intragranular fission-gas bubbles in UO2 fuels with burnup of 6-83 Gwd/T”, Journal of Nuclear Materials 206 (1993) 22-34.

9- White, R.J. “The Development of Grain-Face Porosity in Irradiated Oxide Fuel.” *Journal of Nuclear Materials*, North-Holland, 27 Nov. 2003, www.sciencedirect.com/science/article/pii/S0022311503004616?via=ihub.

10- Setyawan, Wahyu, Michael W. D. Cooper, Kenneth J. Roche, Richard J. Kurtz, Blas P. Uberuaga, David A. Andersson, and Brian D. Wirth. 2018. “Atomistic Model of Xenon Gas Bubble Re-Solution Rate Due to Thermal Spike in Uranium Oxide.” *Journal of Applied Physics* 124 (7): 075107. doi:10.1063/1.5042770.

11- M. Huang, D. Schwen, and R. S. Averback, Journal of Nuclear Materials 399, 175 (2010).

12- J. A. Turnbull and R. M. Cornell, Journal of Nuclear Materials 36, 161 (1970).
13- J. A. Turnbull, C. A. Friskney, J. R. Findlay, F. A. Johnson, and A. J. Walter, Journal of Nuclear Materials 107, 168 (1982).
14- P. Losonen, Journal of Nuclear Materials 304, 29 (2002).
15- M. V. Speight, Nuclear Science and Engineering 37, 180 (1969).
16- https://github.com/ORNL-Fusion/xolotl/wiki/Parameter-File.
17- A. D. Whapham, Nuclear Applications 2, 123 (1966).
18- R. S. Nelson, Journal of Nuclear Materials 25, 227 (1968).
19- R. S. Nelson, Journal of Nuclear Materials 31, 153 (1969).
20- M. S. Veshchunov, Journal of Nuclear Materials 277, 67 (2000).
21- M. S. Veshchunov and V. I. Tarasov, Journal of Nuclear Materials 437, 250 (2013).
22- R. G. Robins, Journal of Nuclear Materials 3, 294 (1961).
23- K. Govers, C. L. Bishop, D. C. Parfitt, S. E. Lemehov, M. Verwerft, and R. W. Grimes, J. Nucl. Mater. 420, 282 (2012).
24- J.A. Turnbull and C.A. Friskney, Journal of Nuclear Materials 71, 238 (1978).
25- C.A. Friskney, J.A. Turnbull, F.A. Johnson, A.J. Walter, and J.R. Findlay, Journal of Nuclear Materials 68 (1977) 186.
26- R.E. Gulden, Journal of Nuclear Materials 23 (1967) 30.
27- M.R. Ruhle, Proc. Conf. on Radiation-induced voids inmetals, New York (1971) p. 255.
28- I.L.F. Ray, H. Rhiele and Hj. Matzke, in: Fundamental Aspect of Inert Gases in Solids, eds. SE. Donnelly and J.H. Evance (Plenum, New York, 1991) p. 457.
29- UNE, Katsumi & KASHIBE, Shinji & TAKAGI, Akira. (2006). Fission Gas Release Behavior from High Burnup UO2 Fuels under Rapid Heating Conditions. Journal of Nuclear Science and Technology - J NUCL SCI TECHNOL. 43. 1161-1171. 10.1080/18811248.2006.9711208.
30- G. Walker (1969), as mentioned by Ref. [12].
31- Philip C. Roth (Oak Ridge National Laboratory), Sophie Blondel (University of Tennessee), David E. Bernholdt (Oak Ridge National Laboratory), Brian D. Wirth (University of Tennessee), “Improving the I/O Performance and Memory Usage of the Xolotl Cluster Dynamics Simulator.” SC Technical Program Publications, 2018.
32- R. M. Cornell and G. K. Williamson, Journal of Nuclear Materials 17 (1965) 200.

33- A. J. Manley, Journal of Nuclear Materials 27 (1968) 244.
34- D. Schwen, M. Huang, P. Bellon, and R. S. Averback, Journal of Nuclear Materials 392, 35 (2009).
35- R. S. Barnes and D. J. Mazey, 3rd European Conf. Electron Miorosoopy (Czech Academy of Sciences, Prague, 1964) 197.
36- R. M. Cornell and G. H. Bannister, Proo. Brit. Ceramic Soe., no. 7 (1967) 365.
37- C.A. Friskney and M.V. Speight, Journal of Nuclear Materials 62 (1976) 89.
38- M. V. Speight, Journal of Nuclear Materials 13, 207 (1964).
39- M. V. Speight and G. W. Greenwood, Phil. Mag. 9, 683 (1964).

VITA

Abdullah Alani was born and raised in Baghdad, Iraq. He moved with his family to Syria in 2006, due to war conditions in Iraq at the time. Then, he resided in Jordan from 2007 until moving to the United States as a refugee in 2012. He has lived in Knoxville, TN ever since.

Abdullah picked up an interest in nuclear engineering while studying at Pellissippi State Community College and was accepted into the nuclear engineering program in the University of Tennessee, Knoxville in 2014. He earned a Bachelor of Science degree in nuclear engineering in 2018, and continued to study at the University of Tennessee, Knoxville as a graduate student in pursuit of a Master of Science degree in nuclear engineering.